# Detailed Observation of Mountain Lee Waves and Comparison with Theory

By
Gene Wooldridge and Peter F. Lester

Department of Atmospheric Science
Colorado State University
Fort Collins, Colorado

Prepared with support under Grant E-10-68G from the
National Environmental Satellite Center ESSA
Project leader: E.R. Reiter
March, 1969

Colorado State University

Department of Atmospheric Science

Paper No. 138

# DETAILED OBSERVATIONS OF MOUNTAIN LEE WAVES AND A COMPARISON WITH THEORY

by
Gene Wooldridge
and
Peter F. Lester

This report was prepared with support under Grant E-10-68G from the National Environmental Satellite Center, ESSA

Project Leader: E. R. Reiter

Department of Atmospheric Science
Colorado State University
Fort Collins, Colorado

March 1969

Atmospheric Science Paper Number 138

## ABSTRACT

A mountain lee wave field study program using satellite photographs, superpressure-balloon trajectories, ground-based cloud photography, and rawinsonde flights is evaluated. The ability of a simple two-layer model to reproduce observed lee wave patterns is tested. The concept of an "effective surface" is introduced to simplify the problem of a complex terrain.

It is observed that shorter and longer wave lengths occur in addition to those predicted by the model. The ability of the model to yield representative amplitudes is greatly affected by the proper selection of the "effective surface" and time changes in the natural airstream.

Satellite photographs have proved to be effective in identifying waves of lengths to sixty kilometers. Wave lengths shorter than six kilometers and billows as small as fifty meters are deduced from the superpressure balloon flights and ground photography.

CONTENTS

LIST OF FIGURES AND TABLES

List of Figures and Tables Continued

List of Figures and Tables Continued

# CHAPTER I

## INTRODUCTION

Orographically induced wave disturbances have been investigated extensively in recent years from both theoretical and observational viewpoints. Observational techniques of a quite varied nature have been employed, in general providing only limited quantitative information.

During the period from October 1967 to January 1968 a number of observational methods were applied to mountain-induced lee waves over eastern Colorado. The various methods were selected because of their capability for looking at a spectrum of scale lengths; that is, wave lengths from tens or hundreds of kilometers to wave lengths of a hundred meters or less. During the four cases presented in this report, an attempt was made to apply all methods simultaneously.

ESSA 6 APT and ESSA 3 video satellite pictures meet the requirement of viewing extensive wave cloud patterns with wave lengths from 4 to 8 kilometers or greater, depending upon location in the photograph. For information on waves of small lateral extent (tenths of km) and of less than a few kilometers in length, a pair of Hasselblad 500 EL cameras was used for stereographic viewing. Radar tracking of transponder-equipped constant-volume balloons spans both the meso- and micro-scale, and was used in conjunction with the ground and satellite photography. The tracks of the balloons are presented here, as well as the power spectra of the balloon tracks. Rawin soundings for the case study days were taken at approximately midway along the superpressure-balloon trajectories to provide information on the vertical structure of the atmosphere. Supplementary soundings are shown for Denver, Grand Junction, and Salt Lake City. Two

of the rawinsonde flights have been analyzed to determine the vertical velocity anomalies from which wave lengths are estimated.

This approach has yielded information on the various wave lengths present in the atmosphere, and the redundancy has given credence to the accuracy of the individual methods of observation.

Further, a brief review of the practical applications of lee wave theory is presented and a simple two-layer model is applied to the terrain and atmospheric conditions of two of the case studies.

# CHAPTER II

## OBSERVATIONAL METHODS

### Satellite Photography

Waves which form over and to the lee of mountainous regions can be viewed and measured on satellite photographs (Fritz, 1965; Neumann, 1967) if they are of sufficient lateral extent, and if sufficient moisture is present for extensive cloud formation in the waves. Wave cloud measurements have found application in the estimation of mean wind speeds when conventional data are scarce or missing altogether (Fritz, 1965). Wave length is best determined by taking a measured distance along a number of waves, and from this determining the length of a single wave.

Lee wave theory anticipates the formation of waves in the lee of mountains in the presence of a stable layer and when the wind at mountain-top levels has an appreciable component perpendicular to the mountain range. When the mountain range has a simple configuration, a single wave length can be expected; however, in the Rocky Mountain region the terrain is complicated, and more than one wave pattern or wave length may result (Fritz, 1965).

In the case studies presented here, not all of the satellite pictures exhibited measurable wave forms over eastern Colorado at the time when waves could be photographed from the ground, due either to lack of sufficient moisture or lack of coherency in the waves. However, there were instances of widespread lee wave cloud patterns over other mountain areas of the western United States coincident in time with the waves over Fort Collins, Colorado, indicating that the general conditions required for formation were present. Thus, from the presence of waves in one part of a mountainous region, it could be inferred that waves existed in another part of the area with similar air mass

characteristics and appropriate wind patterns, but that these waves were not visible in satellite photographs due to low moisture content or smaller wave amplitudes or both.

Photogrammetric Analysis

A photogrammetric analysis of cloud photographs taken from ground locations has been carried out for each of the case study days which are examined in the following section. Two Hasselblad 500 EL cameras were placed on base lines ranging from 3 to 7 kilometers, and pictures were taken synchronously of identical cloud elements. The cameras, equipped with Zeiss lenses with 80 mm focal lengths and 52 degree angles of view, were mounted on transits on which azimuth and elevation could be accurately read. With a knowledge of the exact location of the cameras in a map coordinate system and their altitudes, the position in three-dimensional space of points of cloud elements could be accurately determined (Reiter and Hayman, 1962).

The solution to the photogrammetric equations was made numerically on a CDC 6400 computer available at Colorado State University. The camera sites were chosen individually for each case study so that, in most cases, the camera angle did not deviate more than 30 degrees from a perpendicular to the base line connecting the two cameras. Camera angles greater than 30 degrees from the base lines rapidly increased errors in locating cloud elements in space.

The cloud photographs were mounted on a Haag-Streit comparator, and points on the cloud elements were specified on each photograph and its conjugate mate. Measurements on a cartesian coordinate system attached to the photographs provided data for the computer program. Horizontal and vertical sections of the computed point locations (not

included in this report) yielded the required information on cloud element lengths, and, by suitable interpretation, wave lengths indicated by the clouds themselves.

The photogrammetric analyses gave information on the detailed structure of the atmosphere on the scale of several kilometers to tens of meters. The lower limitation on scale was due mainly to film resolution and the skill of the analyst (Hayman and Peterka, 1963); the upper limit was due to the relatively small field of view of the cameras.

## Superpressure Balloons and Spectral Analyses

During each of the case studies discussed in the next chapter, one or more superpressure-balloon flights were accomplished near a stable layer in the atmosphere. This stable layer was usually found at approximately six kilometers above sea level in the lee of the Rocky Mountains.

The superpressure balloon used was a pillow-shaped Mylar envelope filled with 0.65 cubic meters of helium, and attached to a tow balloon which carried the entire assembly aloft at a rate of about 800 feet per minute (Fig. 1). A fuse in the tether between the two balloons allowed the pillow to separate at a predetermined altitude. A second tether connected a transponder at the base of the pillow balloon. The transponder, which emitted a signal at about 403 MHz, facilitated tracking the assembly.

A pillow balloon seeks to fly at a constant density surface (Booker and Cooper, 1964), has a large vertical drag, and a small restoring force. It therefore slightly underestimates the amplitude of the wave motions in the atmosphere, but in general has proved reliable and is

nsidered to give accurate information on air motion. Horizontal solution was limited in the case studies presented here since the dar determined the position of the balloons only once each minute.

The investigators found one major shortcoming in the use of the perpressure balloons which required serious consideration in the election of field days. The balloons apparently acquired a layer of ce on their exterior during flight through supercooled clouds, causing hem on occasion to descend to the ground. Flights made on cloudless lays or at heights below freezing level encountered no such difficulty (cf. Lally, 1967). In the spectral analyses made of the balloon heights, the data were fitted to a cubic curve by means of least squares to remove trends such as balloon failure and waves of great length from the data.

The vertical representations of the balloon paths are presented in the next chapter of this report. The azimuth and elevation of the balloon were determined by a M33 tracking radar at one minute intervals during flight. The heights of the balloons were computed and subjected to spectral analyses. The smoothed power densities are displayed for each successful balloon flight in the next chapter. One case in which two balloons were flown at nearly the same time and location under very slowly changing conditions allowed two flights to be combined into a single data population, and spectrum analyzed. With the much larger number of data points in this case, pre-whitening of the data could be accomplished without considerable loss of spectral resolution.

The average balloon flight yielded approximately one hundred data points. At a slight loss of confidence level, the time lags were extended to 20% for better frequency resolution of the spectra. This procedure resulted in an average of eight degrees of freedom; that is, there is 80% confidence that the true value lies between 0.60 and 2.3

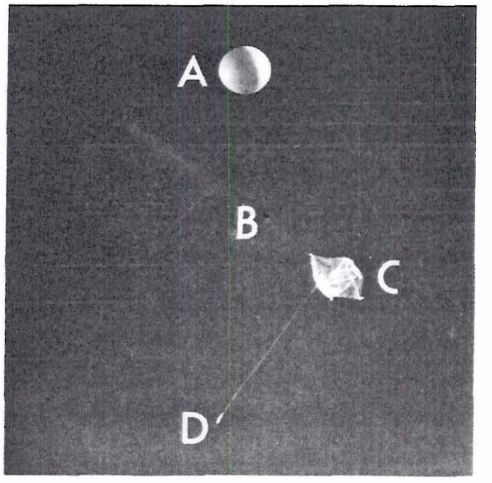


Figure 1. Superpressure Balloon Assembly. The tow balloon A is separated from the pillow balloon C by means of the fuse B in the tether. The transponder D is connected to the pillow balloon by a second tether approximately 10 meters in length.

of the estimate computed (Blackman and Tukey, 1958). The frequencies for the spectra were converted to wave lengths through the use of average horizontal wind velocities for each flight.

Radiosonde Balloon Flights

If vertical motions are sufficiently large, estimates of lee wave properties may be obtained from the ascent of radiosonde balloons using the method proposed by Reid (1952) and Corby (1957). This method also gives additional information on the vertical distribution of the wave features.

Although the radiosonde balloon has not been designed for the measurement of lee wave properties, its response to vertical motions

is adequate for the observation of more pronounced motions. (Corby estimates that vertical motions greater than 1.5 meters per second should be present to use this method.) The method assumes a constant ascent rate of the balloon which may be subtracted out, leaving the vertical motions of the atmosphere and also assumes vertical wave fronts. Two independent sets of data are available for examination from each ascent. First, the radiosonde calibration strip and recorder trace of the flight, and secondly, the radar tracking of the balloon itself. The latter data are found to be highly inaccurate at large distances from the tracking radar. In each case a height-time graph is constructed to which a smooth curve is fitted. Further details of the methods used to analyze these data are found in the references cited above as well as in a study by Andersen (1966).

# CHAPTER III

## FIELD STUDIES

The region of interest for the field studies is shown in Fig. 2. Cases were selected in which the upper flow direction was between 240 and 310 degrees, i.e. generally perpendicular to the predominant mountain ridges of the Front Range in northern Colorado. Balloon flights were tracked by the Ault M33 radar located 16 km east of Fort Collins and rawin soundings were taken at the radar site. Transponder balloon flights were launched from various points in the mountainous region to the west of Fort Collins and at the radar site as shown in Fig. 2. Ground photography was conducted within a 5 km radius of Fort Collins.

### October 26, 1967

The 500 mb chart (Fig. 3b) for 0000 GMT October 27, 1967, showed broad northwesterly flow over the central Rocky Mountains. A surface low pressure center (Fig. 3a) was located over Oklahoma, with an attendant cold front extending westward across the Texas panhandle, New Mexico, and northern Arizona. The radiosonde observation for 2150 GMT October 26, 1967 (not shown) at Ault, Colorado, indicated a marked inversion layer, with its base at 4.7 km MSL and top at 5.4 km MSL. The Denver sounding (Fig. 3c) exhibited the same inversion at 1200 GMT 26 October, with a base at 2.5 km and top at 2.7 km MSL.

Ground-based photogrammetric analyses for the morning of October 26 (Figs. 4a and 4b) placed wave clouds at the base of the Ault inversion layer. A gradual downwind migration of the wave pattern displaced the clouds 5.5 km in 1.4 hours, considerably slower

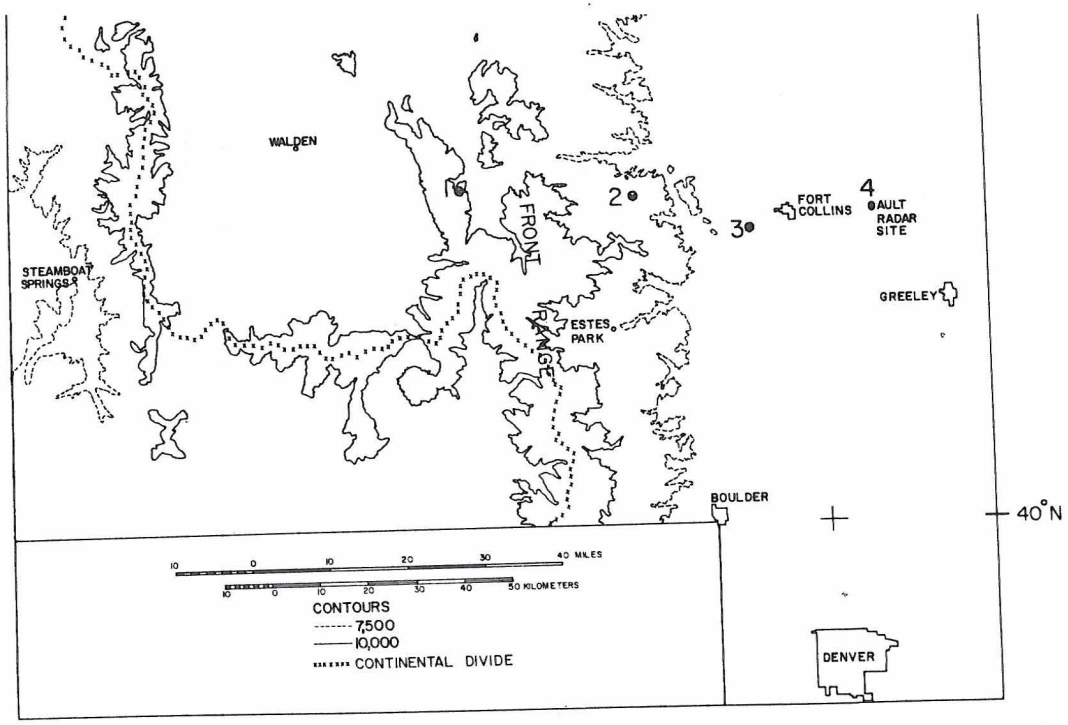


Figure 2. Topographical map of the area over which superpressure balloons were flown. Launch sites are shown as 1, 2, 3, and 4 (also the Ault radar site). Launches were made from site 4 on October 26, 1967, sites 2 and 3 on November 9, 1967, site 2 on November 10, 1967, and site 1 on January 5, 1968.

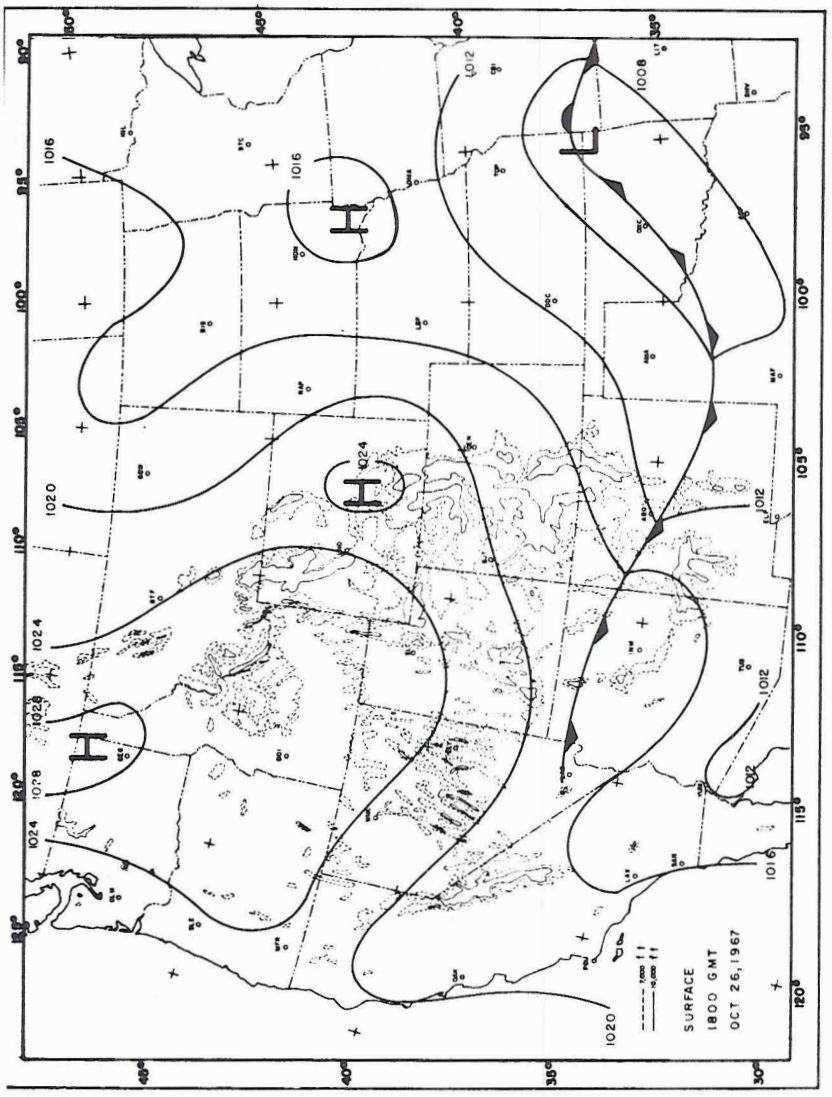


Figure 3a. Surface chart for 1800 GMT October 26, 1967.

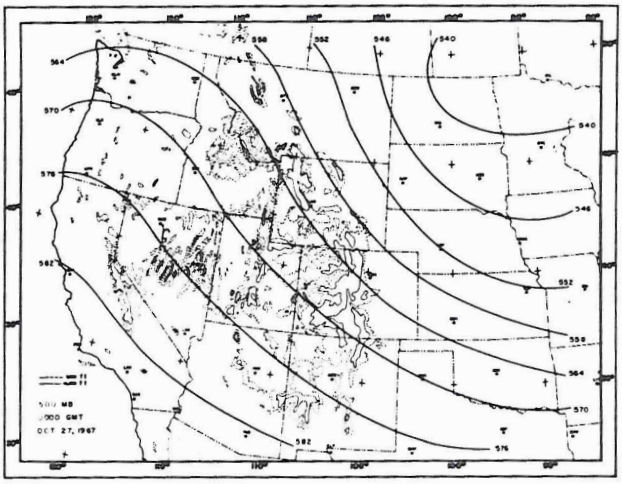

Figure 3b. 500 millibar chart for 0000 GMT October 27, 1967. Heights are in tens of meters.

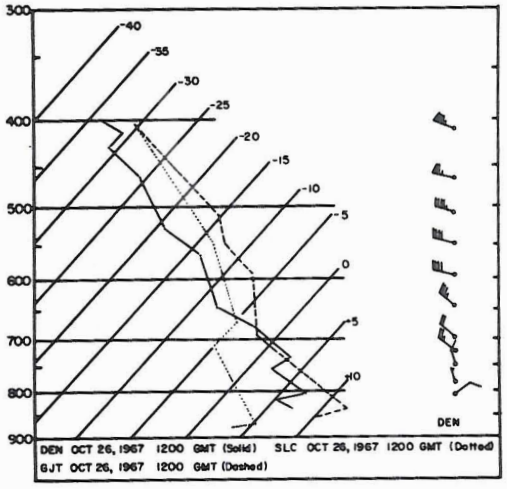


Figure 3c. Soundings for Denver, Grand Junction, and Salt Lake City for 1200 GMT October 26, 1967; on log p, skew T diagram.

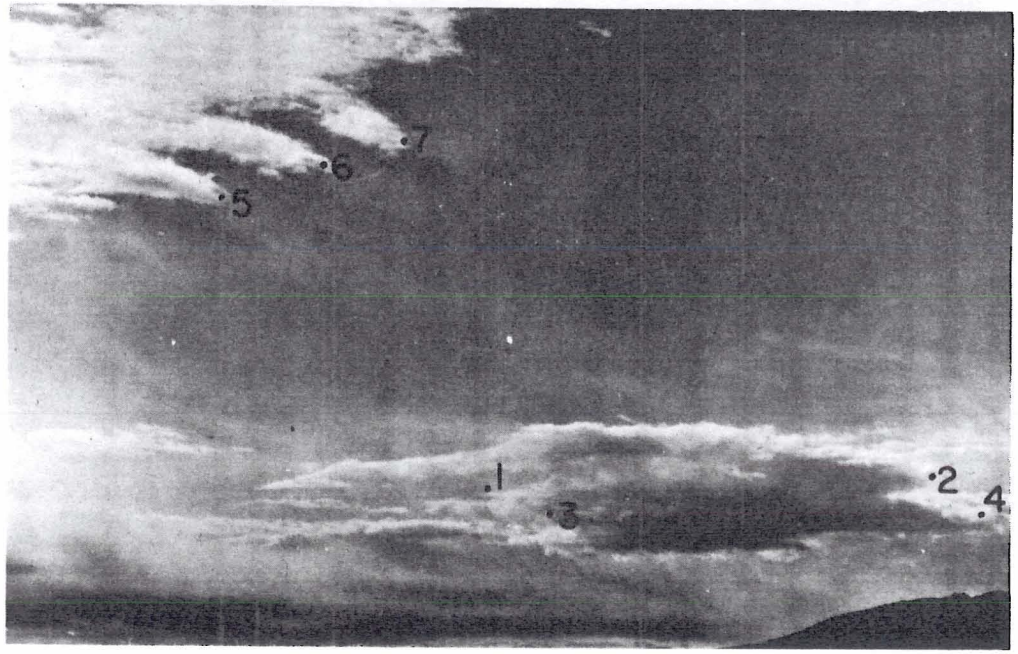


Figure 4a. Ground-based photograph taken at 1625 GMT October 26, 1967. Cloud length (1, 2) is 8.0 km; (3, 4) is 8.5 km; (5, 6) and (6, 7) are 0.5 km.

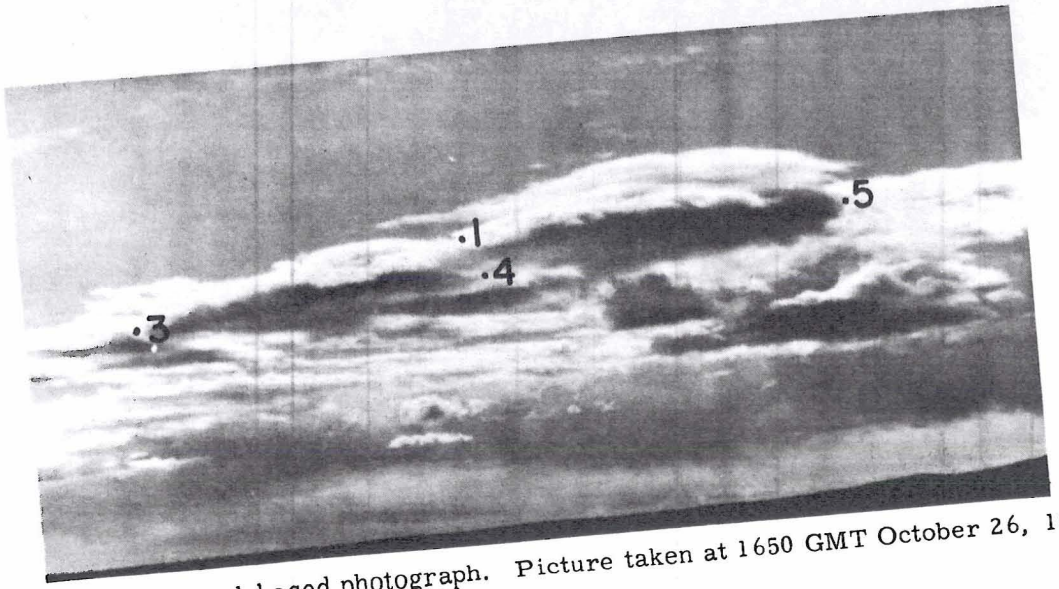


Figure 4b. Ground-based photograph. Picture taken at 1650 GMT October 26, 1967. Cloud lengths (1, 2 and 3, 4) are 4.0 km.

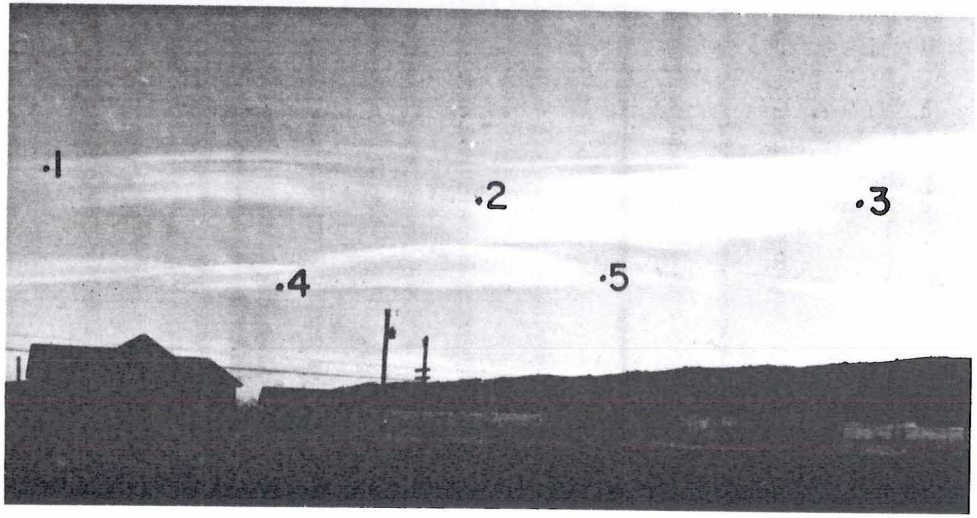


Figure 5a. Ground-based photograph. Picture taken at 2025 GMT October 26, 1967. Cloud length (1, 2) is 7.6 km; (2, 3) is 8.0 km; (4, 5) is 7.0 km.

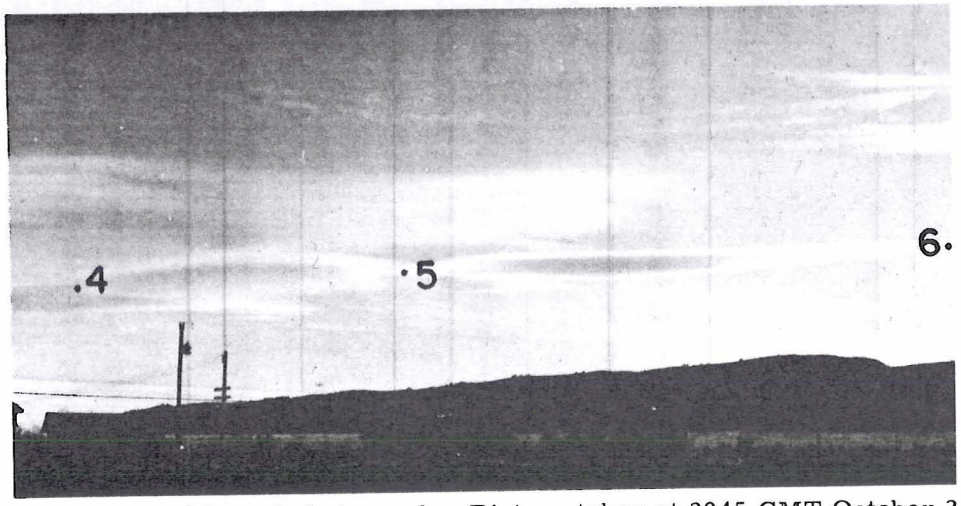


Figure 5b. Ground-based photograph. Picture taken at 2045 GMT October 26, 1967. Cloud length (4, 5) is 7.0 km; (5, 6) is 7.0 km.

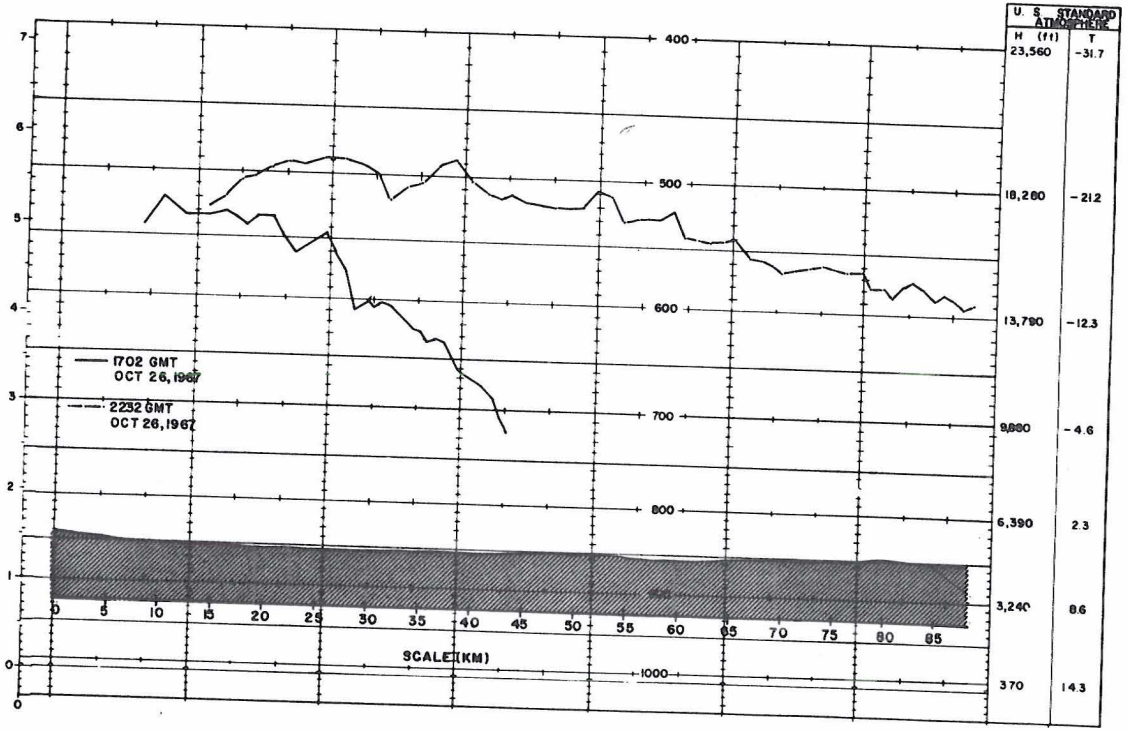


Figure 6a. Superpressure-balloon tracks for October 26, 1967. Points indicate position of balloon at one-minute intervals.

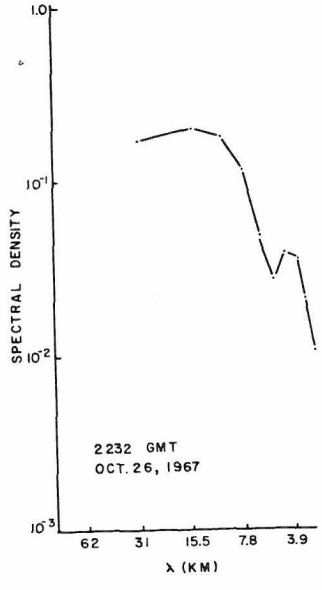


Figure 6b. Spectral analysis of balloon track for 2232 GMT October 26, 1967. Ordinate is in terms of $nF(n)/nF(n)_{max}$.

than the prevailing wind velocity at that level. Wave cloud lengths changed from 8.5 km (Fig. 4a) to 4.0 km (Fig. 4b) during a 25-minute period. Afternoon wave clouds on October 26 (Figs. 5a and 5b) remained essentially fixed in space. Wave clouds were observed at two levels as seen in Fig. 5a. The upper wave train (1, 2, 3 on Fig. 5a) occurred at an elevation of 7.8 km MSL and the lower wave group (4, 5, 6 on Fig. 5b) at 6.7 km MSL in the mean. The wave cloud (1, 2) in Fig. 5a was established at 2005 GMT, and a second cloud (2, 3) had propagated upstream by 2025 GMT. Of the second wave group, the first wave cloud (4, 5), Fig. 5a, was established at 2005 GMT, and the second (5, 6) propagated upstream by 2045 GMT. The wave cloud lengths of the upper wave train were 6.0 km at 2005 GMT, 8.0 km at 2025 GMT, and 7.0 km at 2045 GMT by photogrammetric measurement. The wave cloud lengths of the lower wave group were 8.0 km at 2005 GMT, 7.0 km at 2025 GMT, and 7.0 km at 2045 GMT October 26, 1967.

The vertical representation of the superpressure-balloon flight paths for October 26 is shown in Fig. 6a. The 1702 GMT flight evidently encountered supercooled water in the clouds, iced, and rapidly descended to the ground. The 2232 GMT flight occurred during a period of decreasing cloudiness. Fig. 6b represents the spectral analysis of the height of the 2232 GMT flight indicating a dominant broad peak at approximately 15.5 km and a secondary peak at about 4.5 km.

November 9, 1967

Zonal flow was indicated at midtropospheric levels over the western half of the United States on the 500 millibar chart for 0000 GMT November 10 (Fig. 7b). The surface chart for 1800 GMT November 9 (Fig. 7a) showed a low pressure trough extending from north to south immediately in the lee of the Rocky Mountains, with centers over

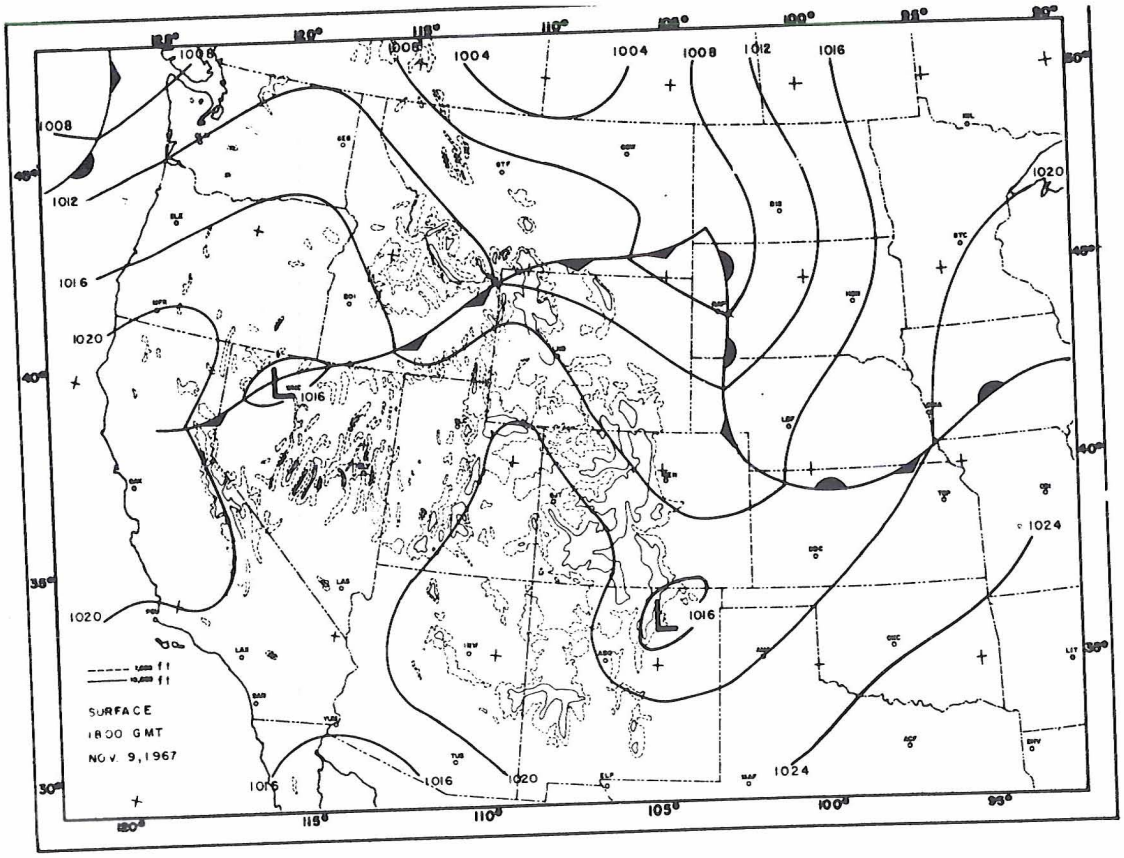


Figure 7a. Surface chart for 1800 GMT November 9, 1967.

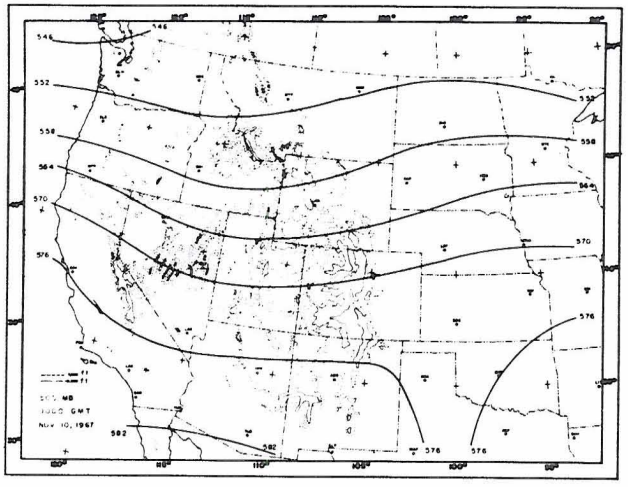

Figure 7b. 500 millibar chart for 0000 GMT November 10, 1967. Heights are in tens of meters.

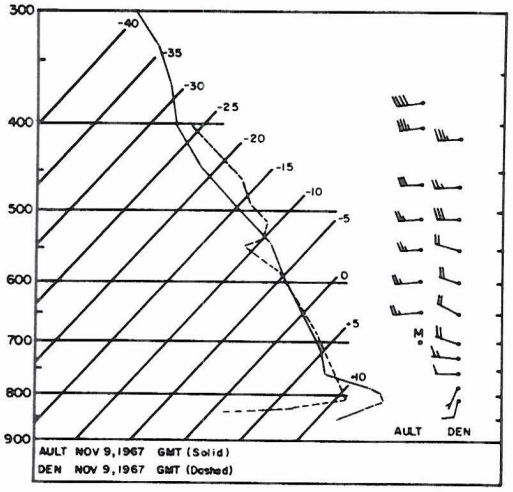


Figure 7c. Soundings for Denver, 1200 GMT November 9, 1967 and Ault, Colorado, 1631 GMT November 9, 1967, on log p, skew T diagram.

extreme southwest North Dakota and northeast New Mexico. The radiosonde observation for Denver at 1200 GMT November 9 (Fig. 7c) contained an inversion based at 5.0 km MSL. Grand Junction did not exhibit this inversion at 0000 GMT November 10 (not shown), but Salt Lake City showed a strong inversion and evidence of a cloud layer near 5.2 km MSL at 0000 GMT November 10 (also not shown). The Ault, Colorado, sounding at 1631 GMT November 9 showed a layer of increased stability from 4.4 to 5.0 km MSL.

The 20:11:17 GMT November 9 ESSA 3 video satellite photograph (Fig. 8a) displayed widespread wave activity over the northwestern United States. Wave lengths measured from wave clouds in the photograph were calculated to be 15 km in central Oregon, 18 km in western Wyoming, 25 km in northern Utah, and 18 km in western Nevada. No extensive wave clouds were seen over Colorado, in keeping with the very low humidities at Grand Junction and Denver.

A single cloud element can be seen over northern Colorado in the ESSA 3 satellite picture (Fig. 8b) taken on the preceding orbit at 18:21:06 GMT November 9. The leading edge of this cloud is estimated to be 40 km east of the Front Range.

The cloud elements measured on the ground-based photographs (Figs. 9a, 9b, 9c and 9d) taken on November 9 were generally of shorter length than those of October 26, 1967. In Fig. 9a, the length of cloud element (1, 2) is 1.9 km, suggesting a wave length of about 2.5 km. A wave cloud two wavelengths in extent is displayed in Fig. 9b as the element (1, 3); the distance (1, 2) is 2.1 km, and (2, 3) is 1.8 km. Cloud element (1, 2) in Fig. 9c is also measured at 1.8 km in length; the billows along the cloud (3, 4) are approximately 50 meters from crest to crest. Fig. 9d includes approximately the

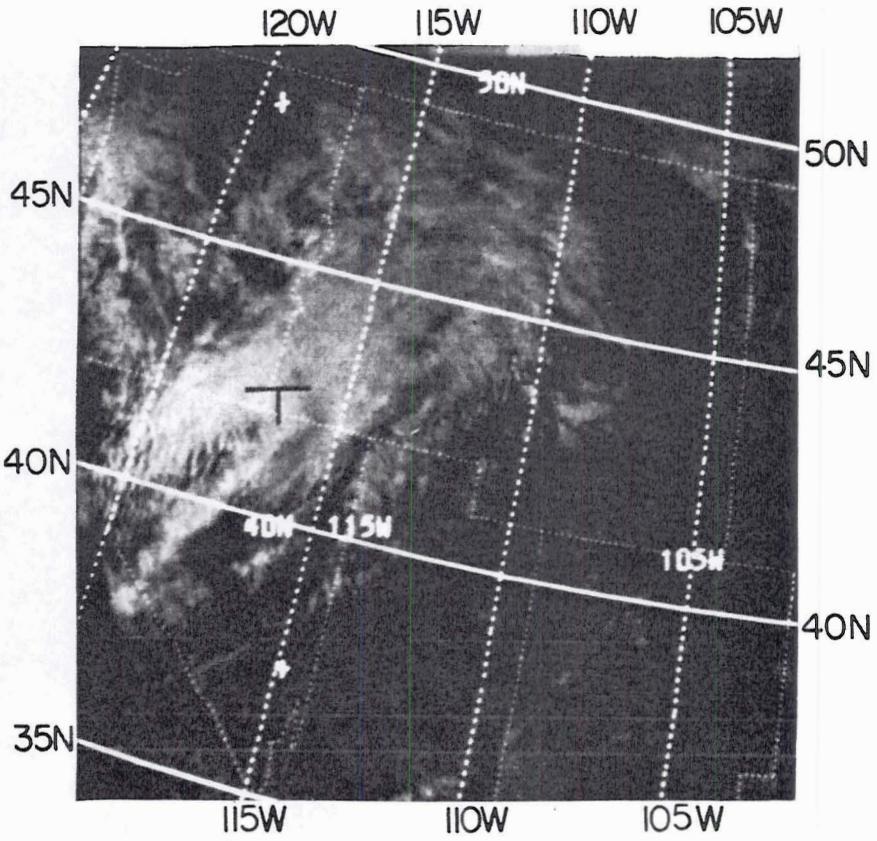


Figure 8a. ESSA 3 video satellite photograph taken at 20:11:17 GMT November 9, 1967.

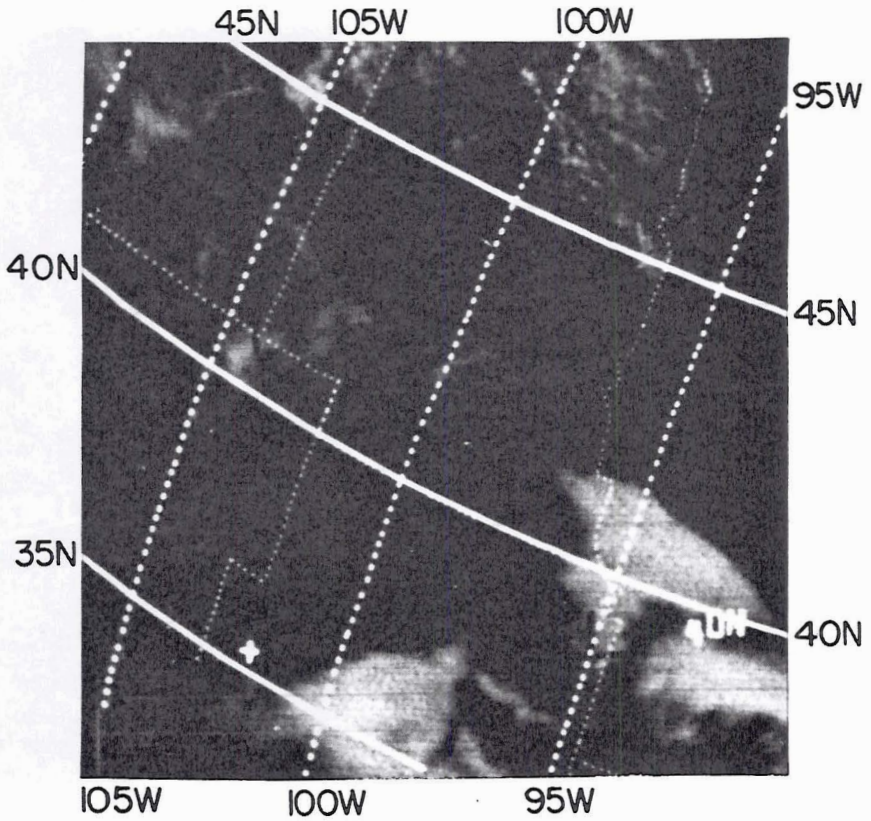


Figure 8b. ESSA 3 video satellite photograph taken at 18:21:06 GMT November 9, 1967.

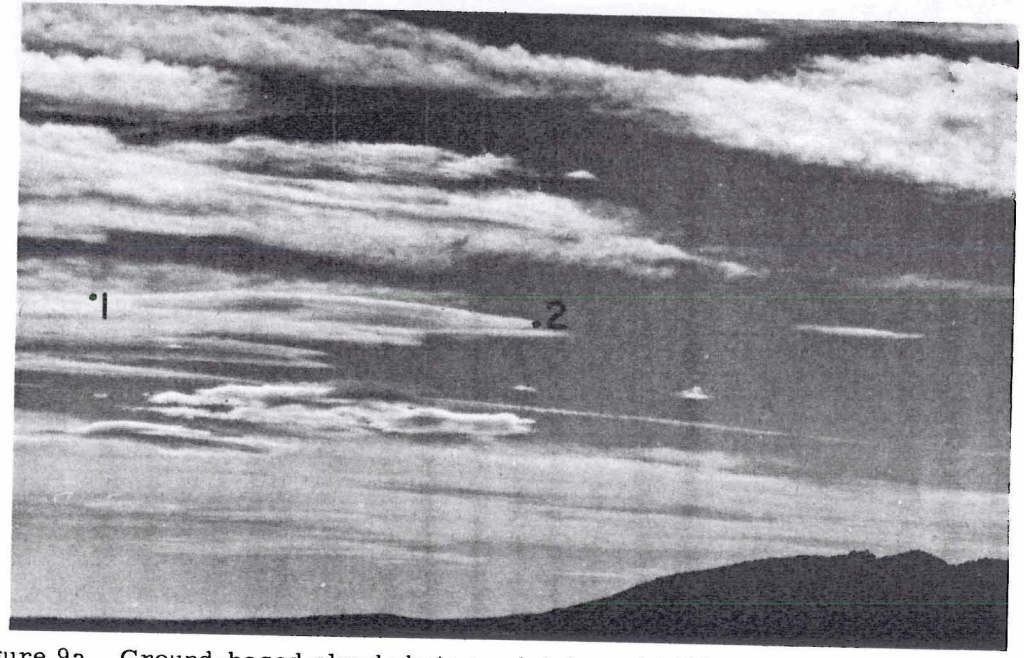


Figure 9a. Ground-based cloud photograph taken at 1800 GMT November 9, 1967.

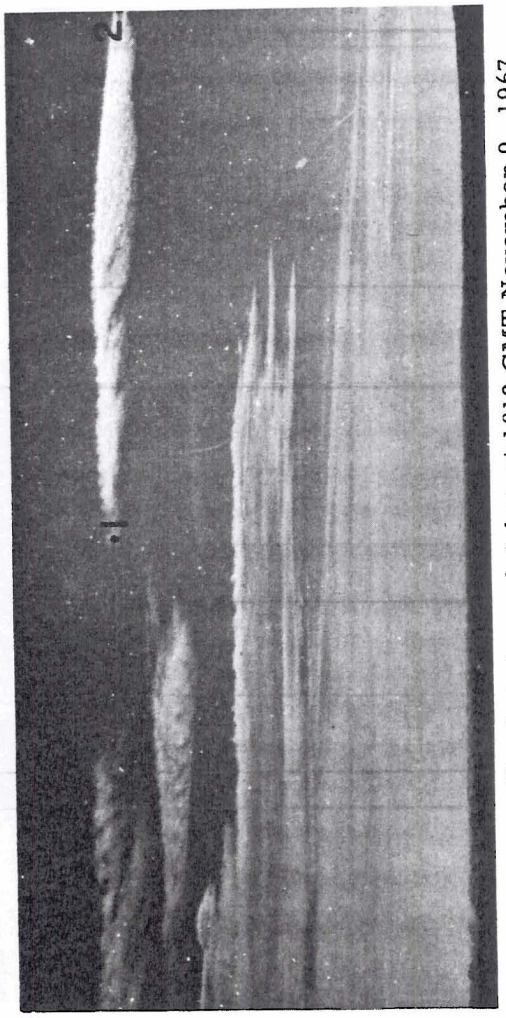

Figure 9b. Cloud photograph taken at 1810 GMT November 9, 1967.

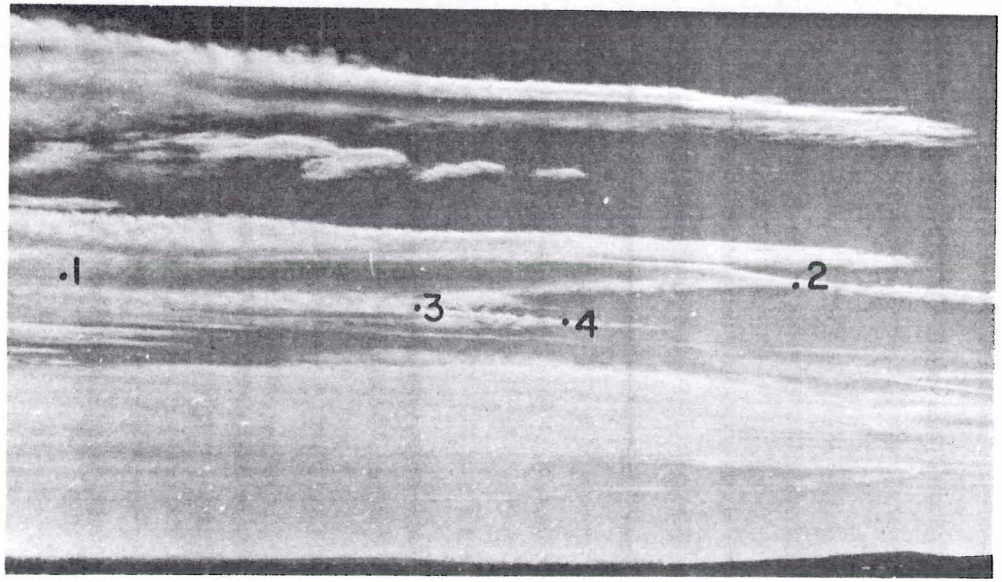


Figure 9c. Cloud photograph taken at 1835 GMT November 9, 1967.

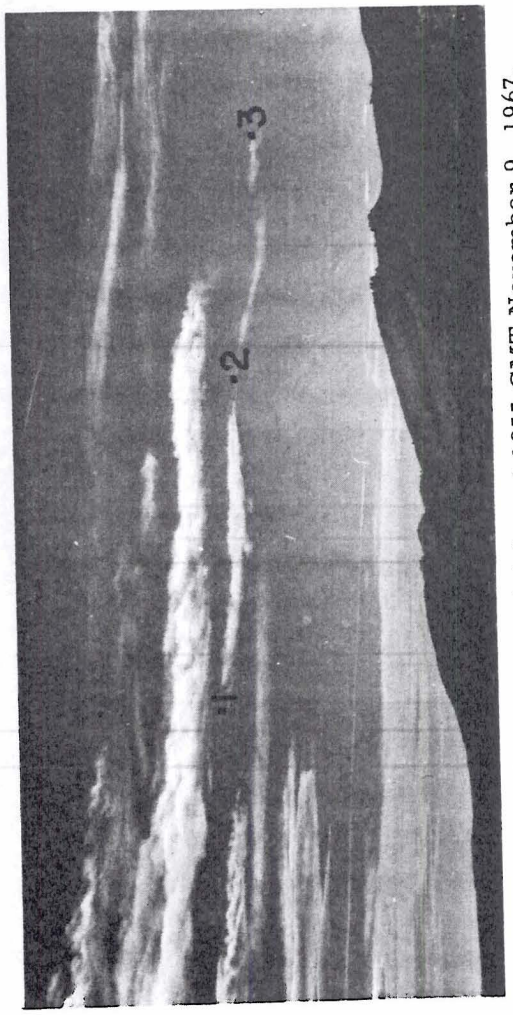


Figure 9d. Cloud photograph taken at 1855 GMT November 9, 1967.

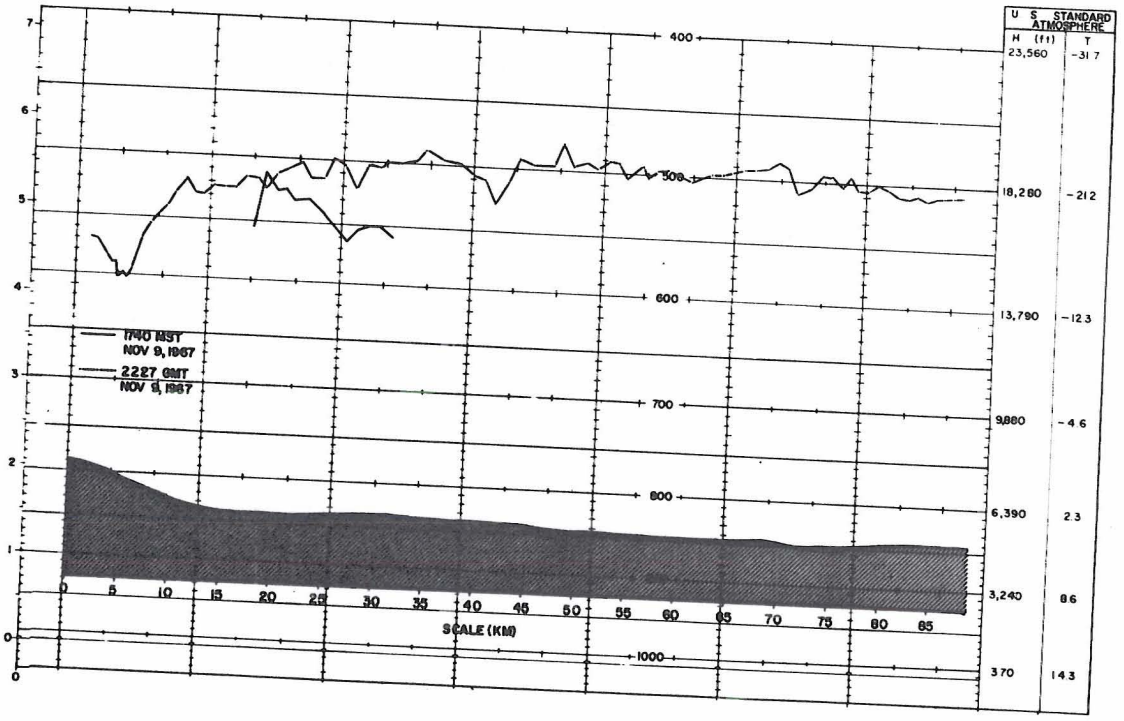


Figure 10a. Superpressure-balloon tracks for November 9, 1967. Points indicate position of balloon at one-minute intervals.

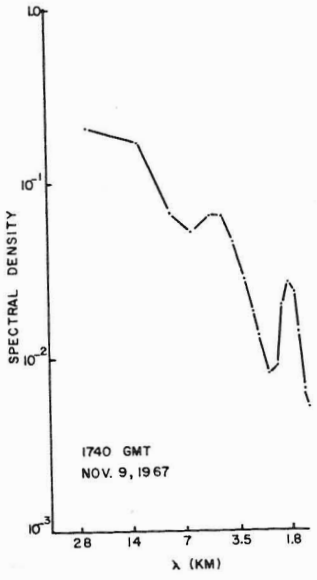


Figure 10b. Spectral analysis for balloon tracks for 1740 GMT November 9, 1967.

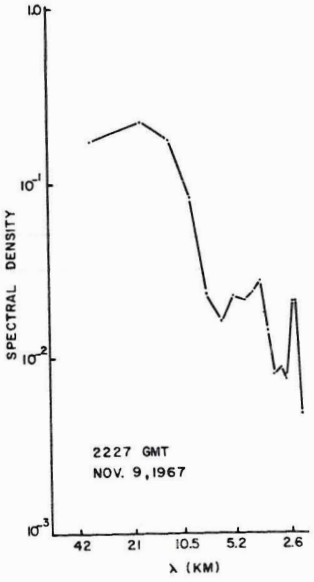


Figure 10c. Spectral analysis for balloon tracks for 2227 GMT November 9, 1967.

same region as Fig. 9c, illustrating the rapid dissipation of the wave clouds. The measured cloud (1, 2) in Fig. 9d is 2.5 km in length.

No definite pattern of downstream migration could be detected through the 55-minute period encompassed by the ground-based photographs. Throughout the period, the apparent wavelengths were on the order of 1.8 to 2.5 km. This sequence of photographs displays dramatically the rapid changes in the lee wave cloud patterns which frequently take place in the area immediately in the lee of the Rocky Mountains.

The 1740 GMT superpressure-balloon flight (Fig. 10a) on November 9 was not successfully tracked near the M33 radar site, and little confidence can be placed in the spectral analysis (Fig. 10b). There is a pronounced secondary maximum at 2.2 km and a weak secondary maximum near 4.6 km, in good agreement with the observed wavelengths drawn from the photogrammetric analyses.

The 2227 GMT November 9 balloon flight was successful (Fig. 10a) and shows only one large vertical motion, in the early part of the flight path. The spectral analysis has its highest peak at 20.5 km, with secondary peaks at 4.3 and 2.6 km. The skies were nearly clear during this second flight and no ground-based cloud photography could be undertaken.

November 10, 1967

The surface trough (see Fig. 11a) which was located in the lee of the Rocky Mountains on November 9 had moved eastward by 1800 GMT November 10 allowing a cold front to pass over eastern Colorado. This front extended from a low pressure center north of Minnesota

southward through Minnesota and northwest Iowa and then southwestward through Nebraska, Kansas, and southern Colorado and Utah. The midtropospheric flow was veering throughout the period, and by 0000 GMT November 11 was from the northwest over the Rockies at 500 mb (Fig. 11b) with velocities increased from approximately 15 m/sec on November 9 to 20 m/sec on November 10.

The radiosonde observation taken at Ault, Colorado, at 1645 GMT November 10 (Fig. 11c) showed a stable layer with its base at 3.6 km and its top at 4.0 km MSL. The Denver sounding at 0000 GMT November 11 (not shown) developed an inversion with its base at 5.7 km and its top at 6.0 km MSL.

Wave clouds were recorded over southwestern Montana on November 10 (Fig. 12a) on the 19:11:30 GMT ESSA 3 video satellite photograph. These clouds were oriented approximately north to south, perpendicular to the 500 mb flow, and wavelengths of about 17 km were measured. Waves could also be seen in the 19:07:10 GMT satellite picture (Fig. 12b) just east of the Front Range in central Colorado and south-central Wyoming, with average wavelengths of 15 km. Additional waves could be seen over northern Utah with wavelengths of 17 km.

An elongated cloud (1, 2, 3 on Fig. 13a) in the 1805 GMT ground-based photograph taken on November 10 measured 14 km in length. There was evidently a shorter length wave imposed on this longer wave; the length (1, 2) was 6.8 km, or very nearly half of the longer wavelength. The cloud (4, 5) in the same photograph was 3.3 km in length. The picture taken at 1840 GMT (Fig. 13b) showed a predominant wavelength of approximately 6 km; the cloud (1, 2) measured 5.5 km, the cloud (3, 4) measured 6.6 km, and the cloud (5, 6) measured 6.1 km.

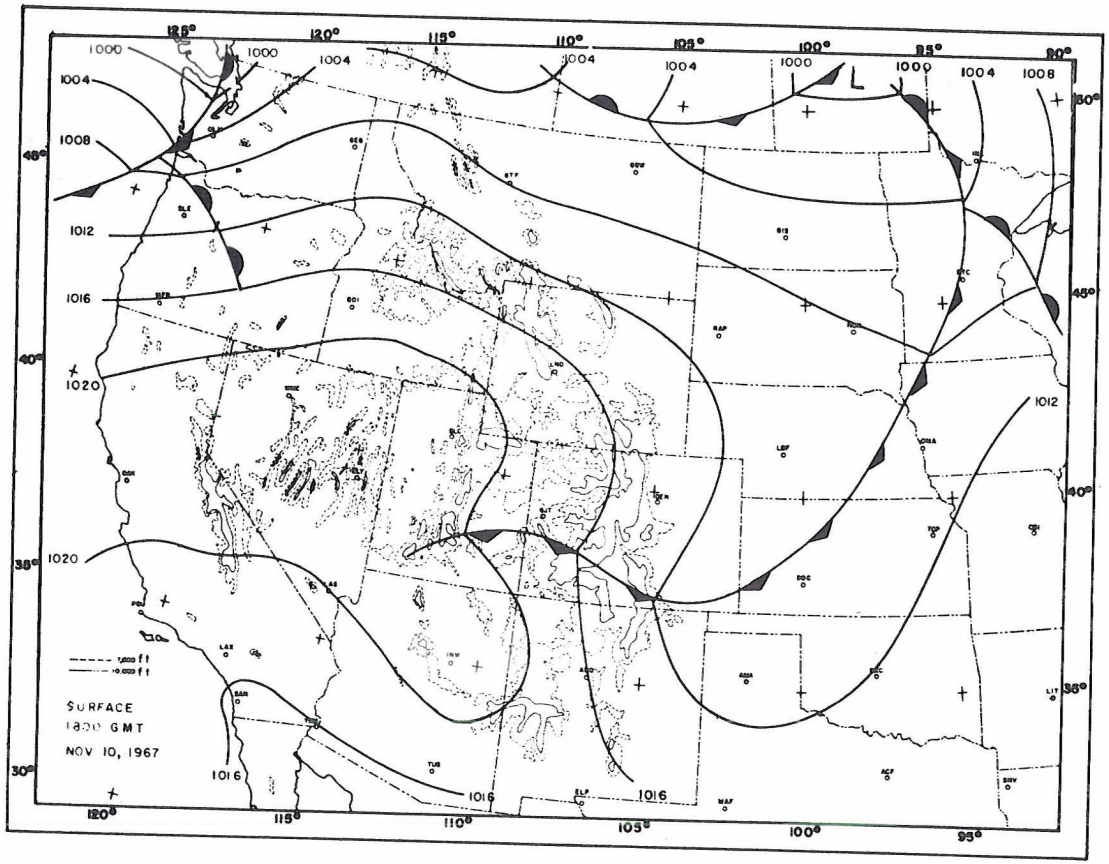


Figure 11a. Surface chart for 1800 GMT November 10, 1967.

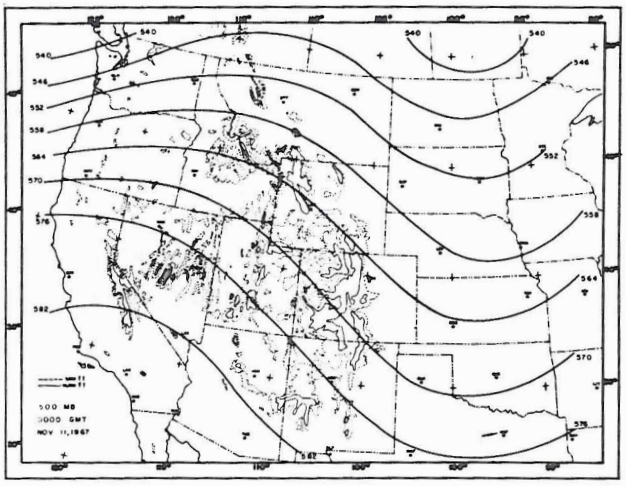

Figure 11b. 500 millibar chart for 0000 GMT November 11, 1967. Heights are in tens of meters.

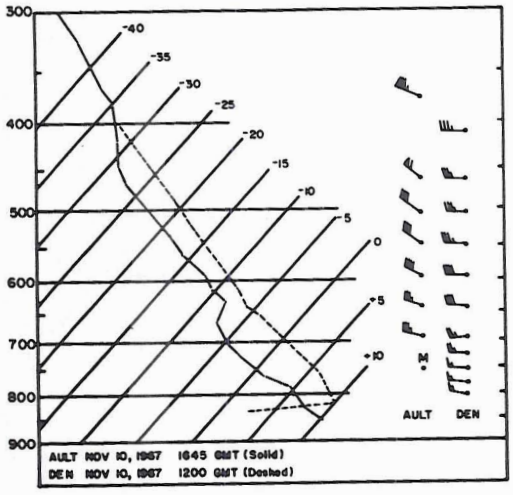


Figure 11c. Soundings for Ault, Colorado, 1645 GMT November 10, and Denver 1200 GMT November 10, 1967, on log p, skew T diagram.

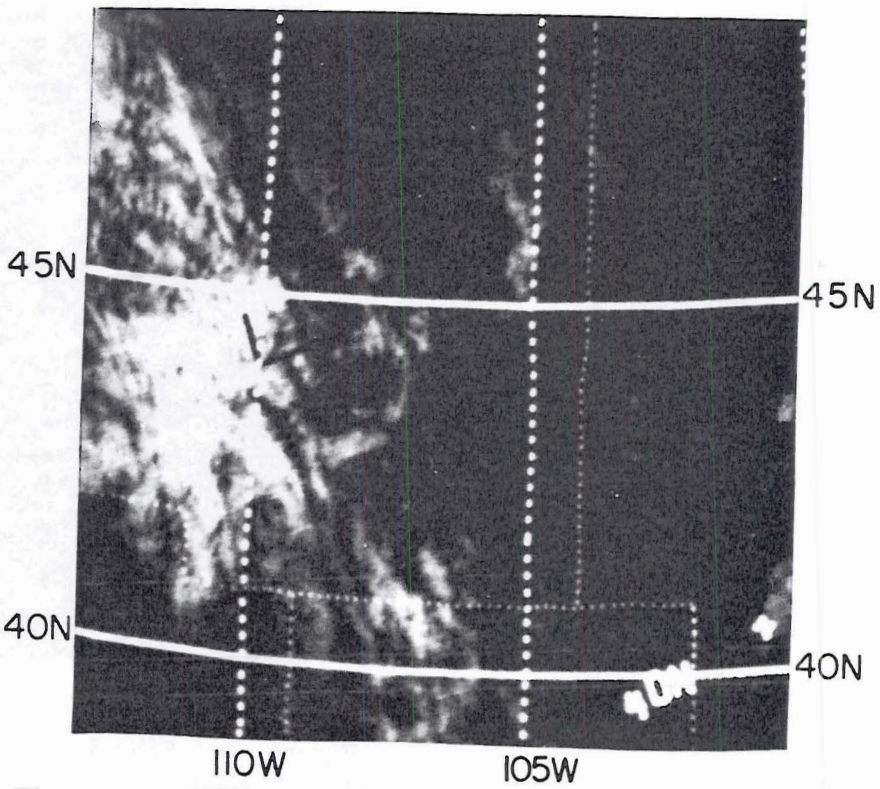


Figure 12a. ESSA 3 satellite photograph taken at 19:11:30 GMT November 10, 1967.

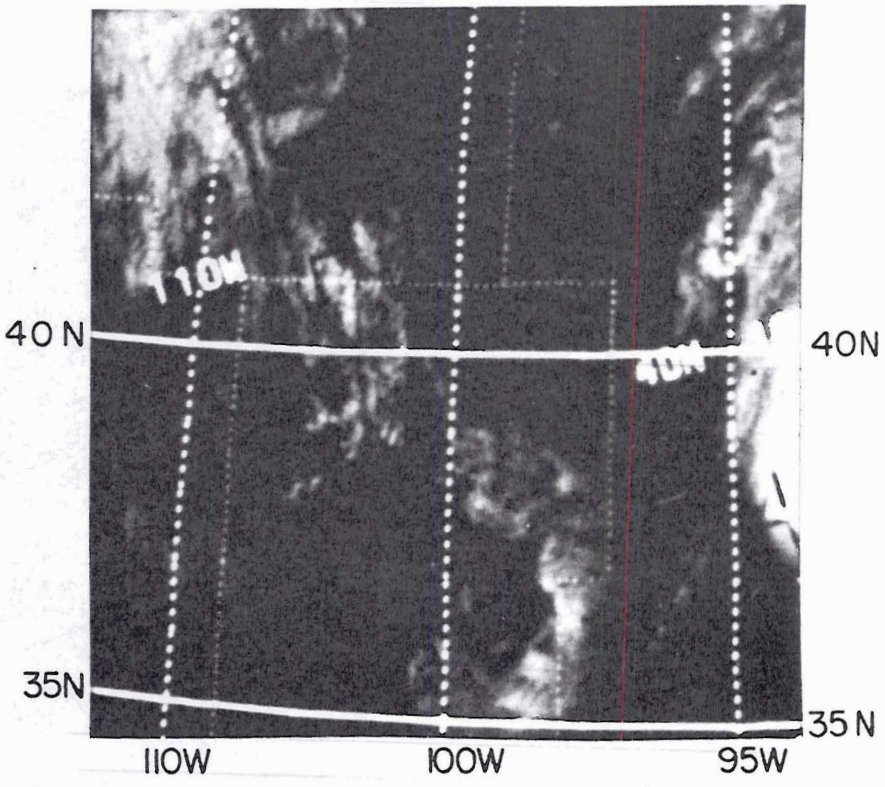


Figure 12b. ESSA 3 satellite photograph taken at 19:07:10 GMT November 10, 1967.

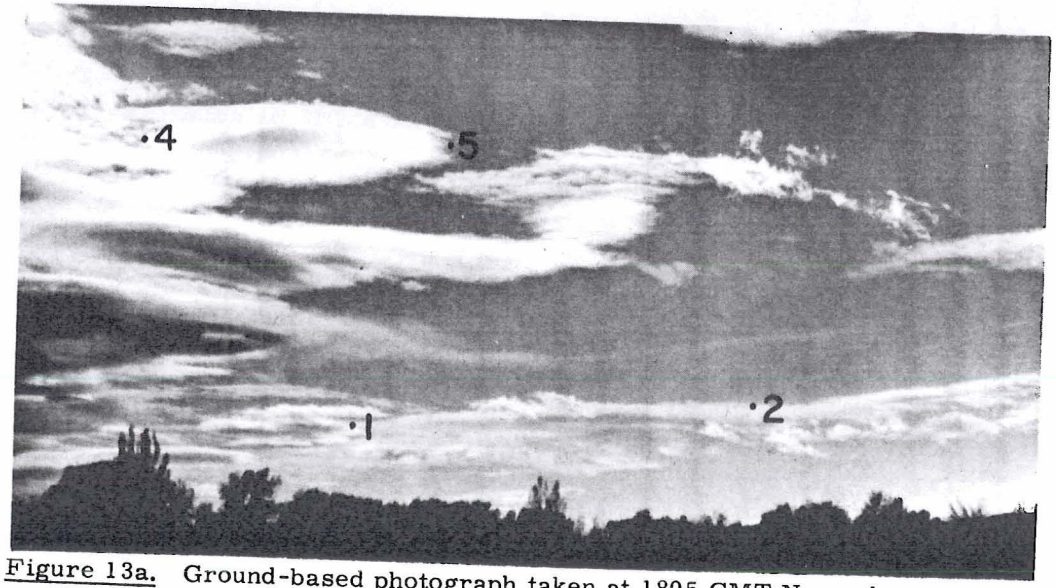


Figure 13a. Ground-based photograph taken at 1805 GMT November 10, 1967.

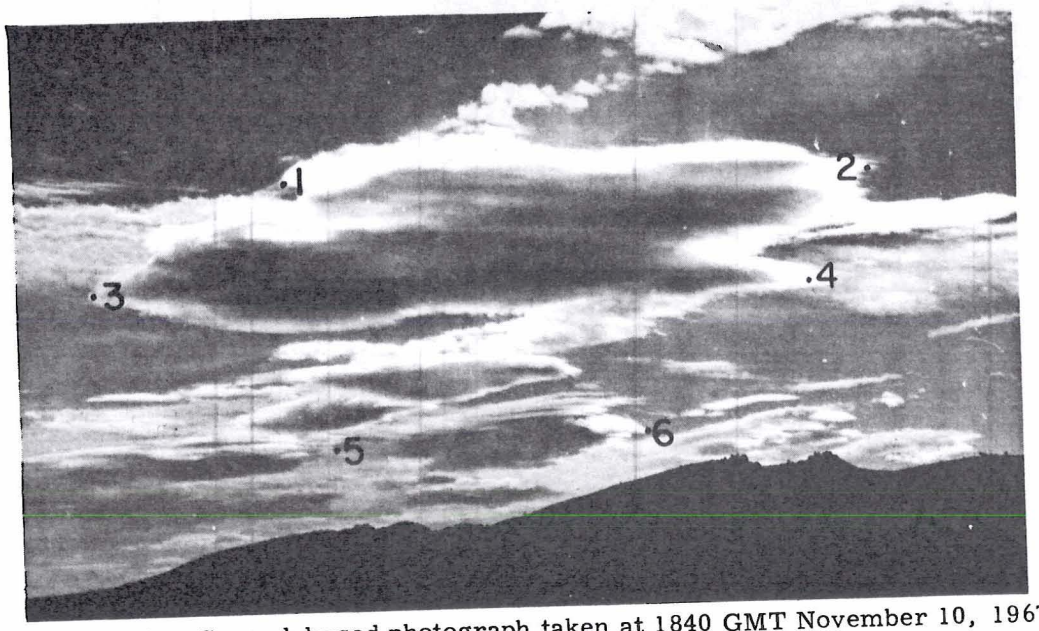


Figure 13b. Ground-based photograph taken at 1840 GMT November 10, 1967.

The individual cloud axes remained nearly perpendicular to the Front Range throughout the period. The height of the clouds (5.8 km MSL) agreed with the height of the base of the stable layer found on the 0000 GMT November 11 Denver sounding (not shown).

The 1735 GMT November 10 superpressure-balloon flight (Fig. 14a) showed extreme vertical motions during its initial few kilometers, followed by an irregular wave pattern, and finally by what appeared to be balloon failure. The spectral analysis of the flight (Fig. 14b) showed small peaks at 8.3 and 3.8 km, but the flight path was of insufficient length to resolve the low-frequency end of the spectrum. The 2037 GMT flight (Fig. 14c) was more successful, exhibiting a broad peak centered at about 20 km and a second peak at 5 or 6 km.

From the rawinsonde balloon ascent at 1939 GMT a predominant wavelength of approximately 16 km is observed with the maximum amplitude occurring in the range between 3.5 and 5.0 km MSL (Fig. 4d). A secondary wave of about 4 km length is also found.

anuary 5, 1968

The 1800 GMT surface chart for January 5, 1968 (Fig. 15a) contained an inverted trough extending from western Texas northward through eastern Colorado, then northwestward through central Wyoming nd eastern Idaho. Two closely spaced cold fronts extended from Iowa estward through southern Nebraska into the trough in Wyoming and aho. Low pressure centers were located over the Texas Panhandle, rtheastern Colorado, and eastern Idaho. The 500 mb flow at 0000 MT January 6, 1968 (Fig. 15b) was westerly over the eastern Rocky ountains and over the plains states to the east.

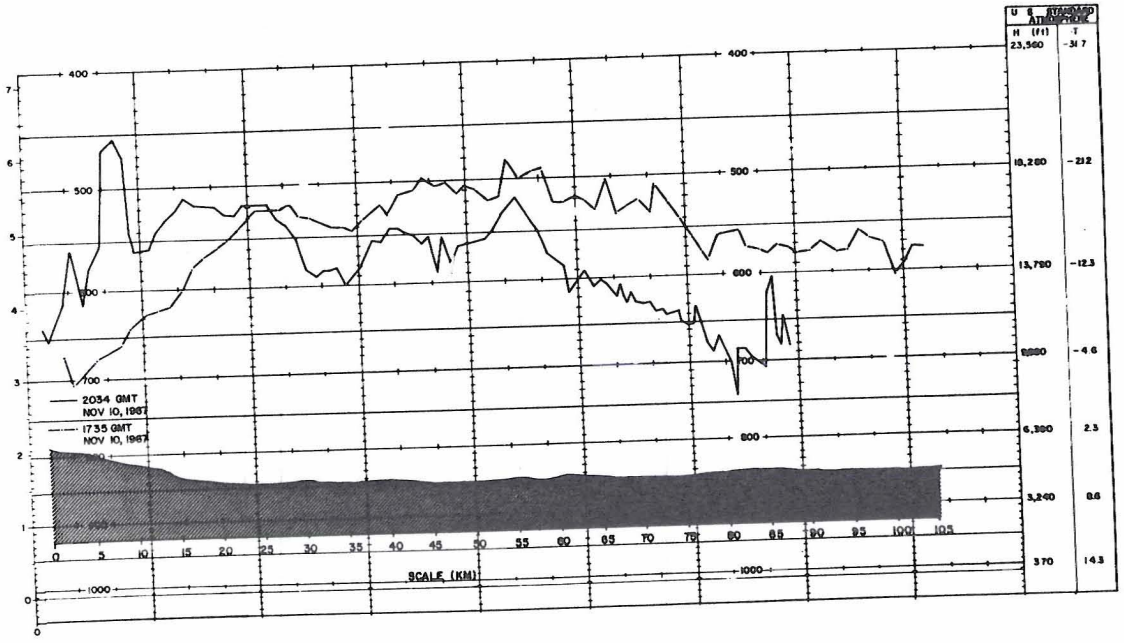


Figure 14a. Superpressure-balloon heights for 1735 GMT and 2037 GMT November 10, 1967.

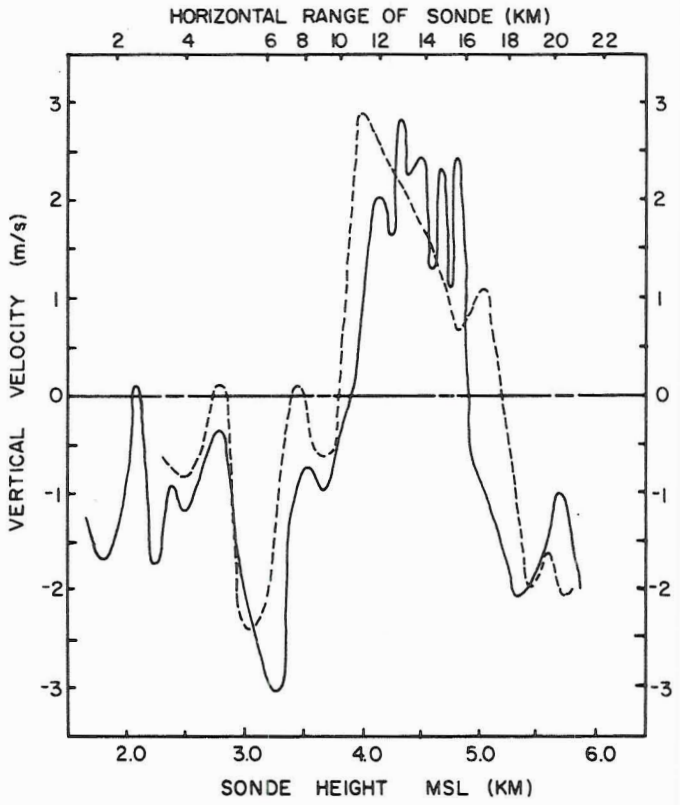


Figure 14d. Analysis of 1739 GMT November 10 rawinsonde balloon ascent. The dashed line is from analysis of radiosonde data; the solid line from analysis of radar data.

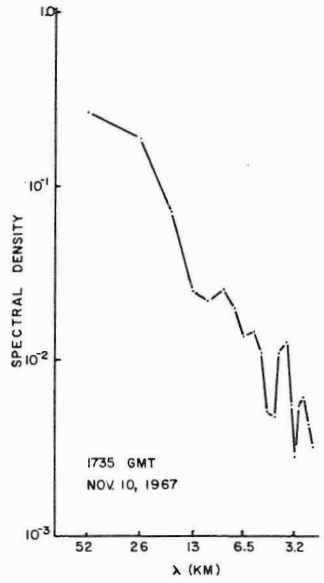


Figure 14b. Spectral analysis for 1735 GMT November 10, 1967 superpressure-balloon flight.

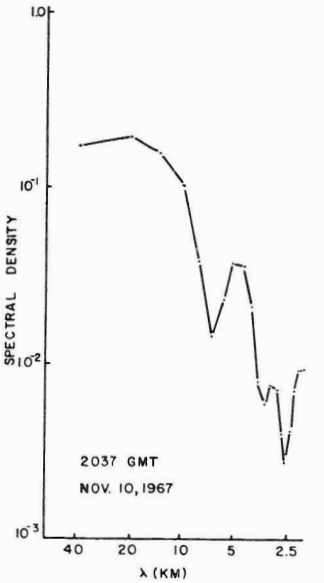


Figure 14c. Spectral analysis for 2037 GMT November 10, 1967 superpressure-

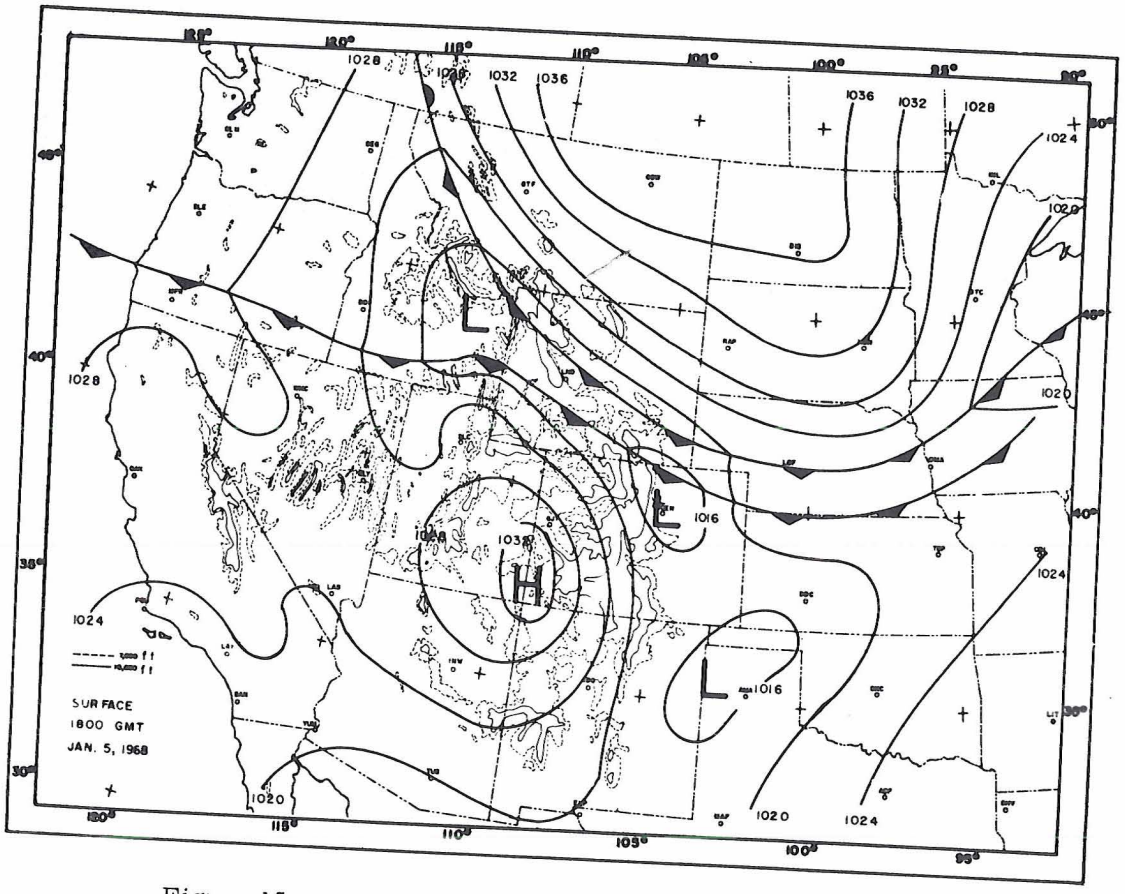


Figure 15a. Surface chart for 1800 GMT January 5, 1968.

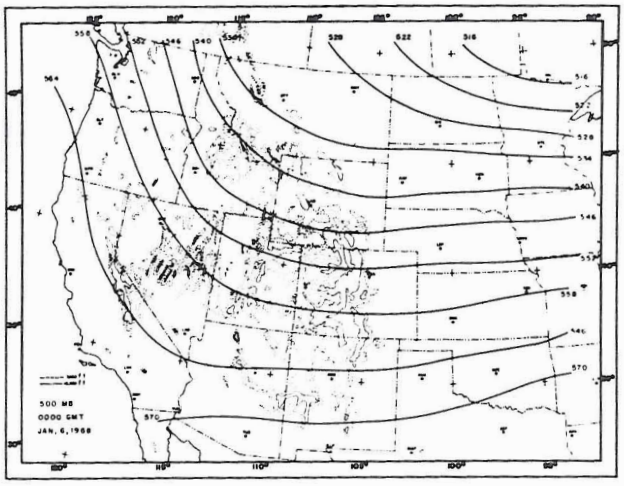


Figure 15b. 500 millibar chart for 0000 GMT January 6, 1968. Heights are in tens of meters.

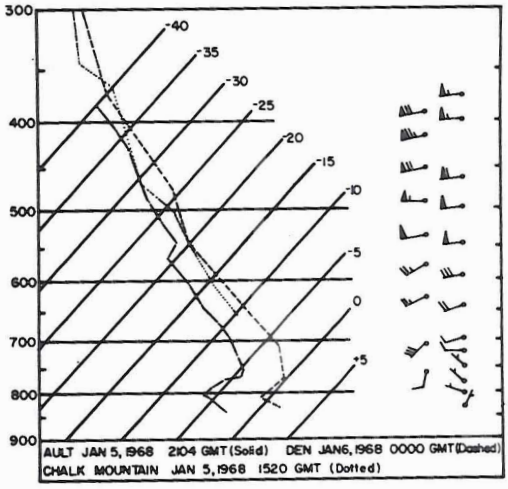


Figure 15c. Soundings for Ault, Colorado, 2104 GMT January 5, 1968, Denver 0000 GMT January 6, 1968, and Chalk Mountain, Colorado; on log p, skew T diagram.

The 2104 GMT January 5 radiosonde observation for Ault, Colorado, showed a stable layer with a base at 4.7 km and top at 5.0 km MSL (Fig. 15c). This stable layer was not present on the Denver 0000 GMT January 6 sounding, but was found on the 0000 GMT January 6 Salt Lake City sounding (not shown), with a base at 4.4 km and top at 5.0 km, together with a higher stable layer with a base at 6.0 km and top at 6.6 km.

The ESSA 3 video satellite picture (Fig. 16a) showed the leading edge of a widespread wave cloud at 105.5°W from 39°N to 41° N. This cloud was observed from the ground as a sharp edge running from north to south, beginning just west of Fort Collins, Colorado, and extending eastward to the horizon. A persistent cap cloud was also observed from the ground between 1530 GMT and 2000 GMT January 5 from the balloon launching site at Chambers Lake (site 1, Fig. 2). The clear area seen in the ESSA 3 18:24:38 GMT photograph between the cap cloud and the edge of the wave cloud measured about 55 km on the basis of ground and satellite observations. No ground-based photographs were taken on this day, so the height of these clouds could not be fixed. The weather observation taken at Colorado State University for 1800 GMT January 5 estimated the cloud there at about 15,000 ft MSL. The cap cloud over the Front Range extended down to the surface at the mountain ridge.

Three superpressure-balloon flights were launched on January 5, 1968 from Chambers Lake (site C, Fig. 2). The first two were launched nearly simultaneously to fly at approximate mean pressures of 550 mb 1612 GMT) and 470 mb (1603 GMT), emitting slightly different transponder frequencies for identification by the radar personnel. These balloons (Fig. 17a) underwent considerable vertical displacements during their flights, and the lower balloon apparently failed late in its

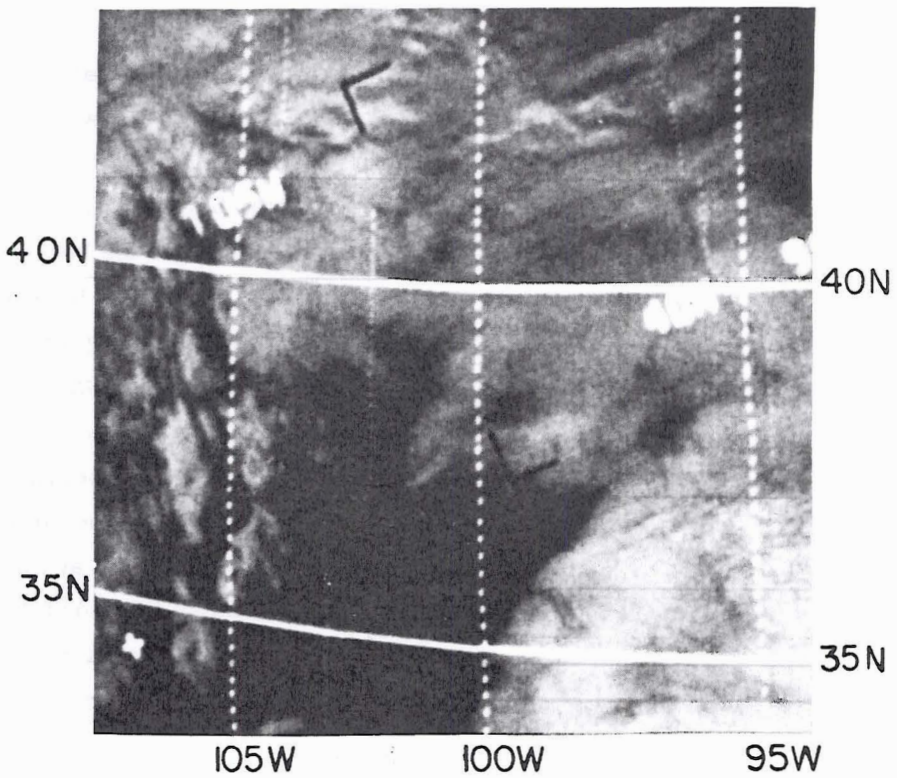


Figure 16a. ESSA 3 satellite photograph taken at 18:24:38 GMT January 5, 1968.

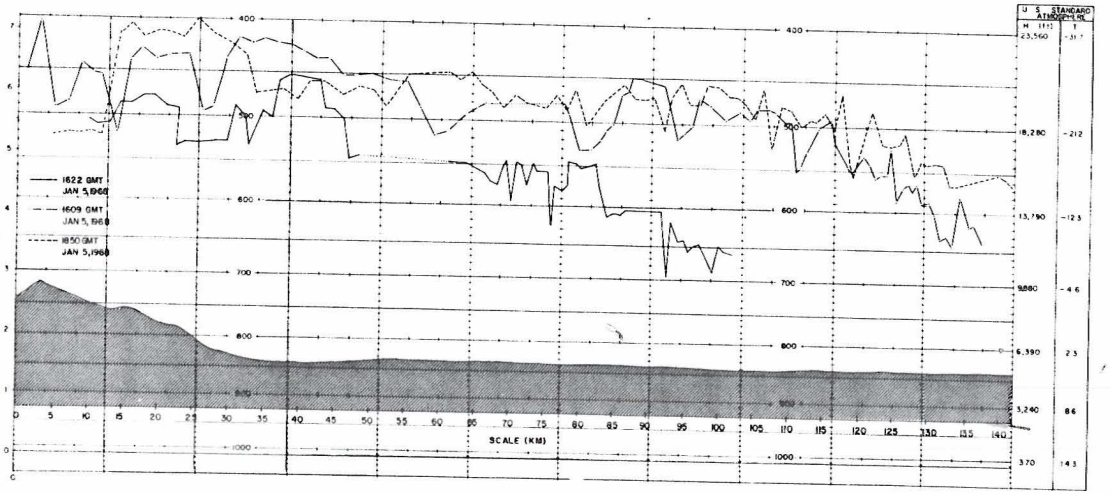


Figure 17a. Superpressure-balloon heights for 1609 GMT, 1622 GMT, and 1850 GMT January 5, 1968.

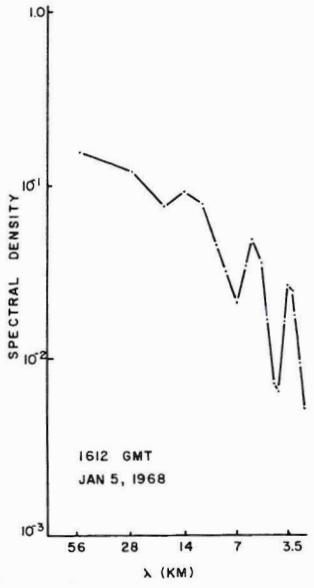


Figure 17b. Spectral analysis for 1612 GMT January 5, 1968 superpressure-balloon flight.

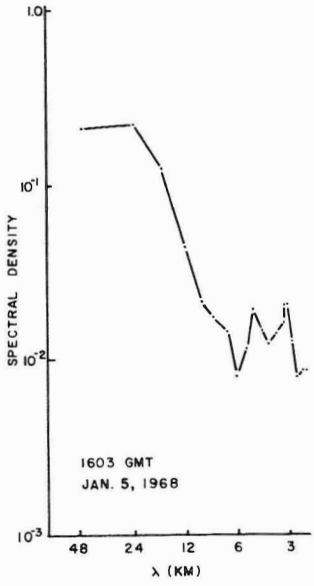


Figure 17c. Spectral analysis for 1603 GMT January 5, 1968 superpressure-balloon flight.

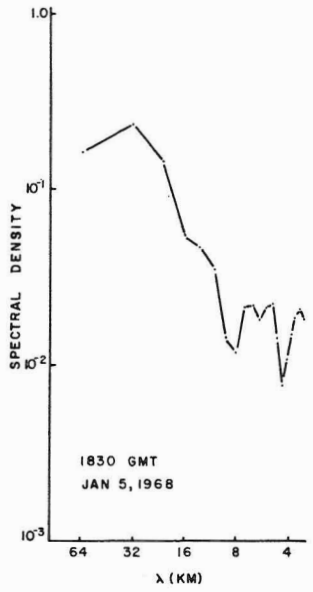


Figure 17d. Spectral analysis for 1830 GMT January 5, 1968 superpressure-balloon flight.

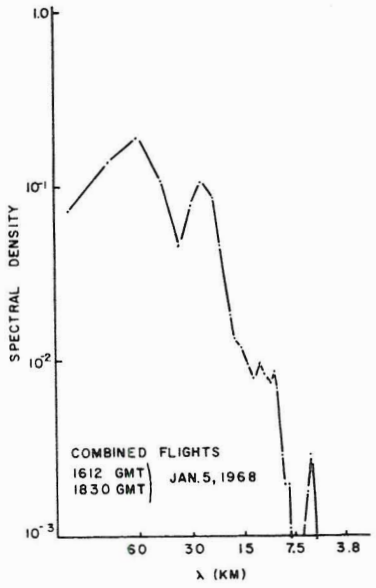


Figure 17e. Spectral analysis for combined 1612 GMT and 1830 GMT January 5, 1968 superpressure-balloon flight.

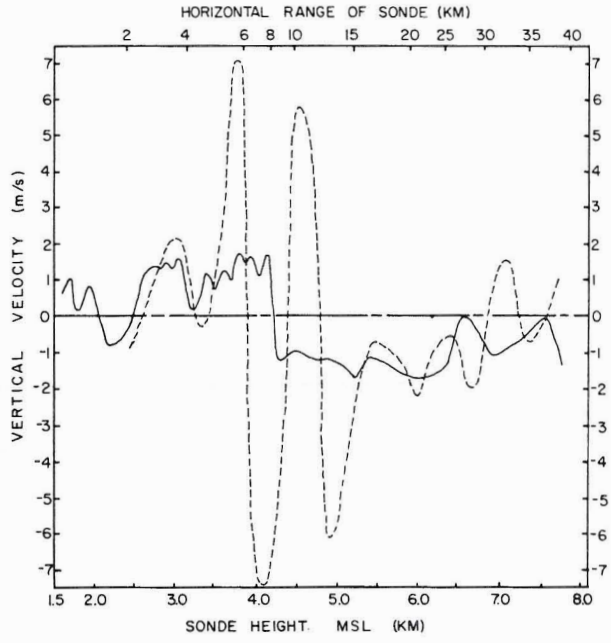


Figure 17f. Analysis of 2104 GMT January 5, 1968 rawinsonde and radiosonde flights. The dashed line is from analysis of radiosonde data; the solid line from analysis of radar data.

flight. The third balloon (1830 GMT) was released to fly at about 470 mb. There was reasonable agreement on the large-scale flow patterns between the first two flights and on the first part of all three flights (Fig. 17a).

The spectral analysis of the lower flight (1603 GMT, Fig. 17b) exhibited a broad peak at low frequency centered at about 24 km, and lesser peaks at 5.5 km and 3.2 km wave lengths. The spectral analysis of the 1612 GMT flight (Fig. 17c) showed peaks at about 14 km, 6.3 km, and 3.5 km wave lengths. The second 470 mb flight (Fig. 17d) contained a peak at 32 km and a broad band centered at about 6.0 km. The data from the two higher balloon flights have also been combined into a single data population for spectral analysis. The combined 470 mb flights (Fig. 17e) exhibited maximum densities at 60 km and 27 km, with a peak at about 6.0 km.

Analysis of the 2104 GMT rawinsonde flight shows two predominant wave features corresponding to wavelengths of about 4 km and 33 km with the greatest amplitudes observed at heights between 3.5 and 5.0 km MSL (Fig. 17f). The large variation between radiosonde and radar estimates could not be explained.

# CHAPTER IV

# OBSERVED AND COMPUTED LEE WAVE CHARACTERISTICS

## A. Introduction

In the last section of this report, the feasibility of the nearly simultaneous observations of atmospheric motion on various scales has been examined in detail. One basic aim of such a study is to determine the scales of motion capable of being seen both "explicitly" and "implicitly" by a satellite. An implicit observation requires an understanding of the physical relationship between the explicit or directly observable state of the atmosphere and the smaller scales of motion which are not directly observable. It is the purpose of this portion of the report to describe some initial steps that have been taken toward defining relationships of the type just described, particularly with respect to lee wave activity.

## B. Literature Review

The theoretical aspect of mountain waves has been investigated in detail particularly over the past 25 years. Comprehensive reviews of the subject have been given by Corby (1954) and Krishnamurti (1964). The important result of these studies is that realistic systems of lee waves have been reproduced via simple mathematical models. Further, the important roles played by various physical parameters such as vertical wind shear, static stability and mountain size and shape in the development of lee waves have been quantitatively verified.

The possibility of utilizing these mathematical models to relate observed lee wave characteristics to the state of the atmosphere has

been attempted by many investigators. A brief summary of some of these attempts is given below.

Corby (1957) has demonstrated empirically that the mean tropospheric wind speed is related linearly to the lee wave length. Foldvik (1962) has performed a rather comprehensive study of some 26 lee wave cases. Utilizing a two-dimensional, single-layer lee wave model similar to that of Palm and Foldvik (1960), he found good correspondence between observed and computed wave lengths and vertical velocities, thus indicating that a relatively simple model is capable of approximating the state of the atmosphere under lee wave conditions.

The ability of meteorological satellites to resolve lenticular cloud forms has been well-established (e. g. see Conover, 1964; Widger, Sherr and Rogers, 1965). Since lenticular clouds are visual manifestations of wave activity, investigators have been prompted to relate characteristic dimensions of the satellite-observed wave clouds to atmospheric conditions.

Döös (1961, 1962) has applied a two-dimensional model in the analysis of lee wave clouds photographed in the lee of the Andes by TIROS I. He found that the theoretical calculations of lee wave lengths were comparable with the observed wave lengths.

Fritz (1965) has shown that a good estimate of the mean tropospheric wind speed can be computed from the relationship

$$\lambda = \bar{u} \frac{2\pi}{\sqrt{gs}} \qquad (1)$$

where $\lambda$ is the lee wave length measured from satellite pictures,

$\bar{u}$ is the mean tropospheric wind speed,

| | | |
|---|---|---|
| | $g$ | is the acceleration due to gravity, |
| | $s = \frac{1}{\theta} \frac{\partial \theta}{\partial z}$ | is the mean stability of the troposphere, |
| | $\theta$ | is potential temperature, |
| and | $z$ | is the vertical coordinate. |

By assuming some mean stability Fritz found good correspondence between observed and computed values of $\bar{u}$. Only in the case where stability changed rapidly with time on the synoptic scale was the comparison poor. This method may be inverted, i. e. knowing $\lambda$ and $\bar{u}$, the mean stability may be found. Equation (1) is based on simple parcel theory.

Anderson (1966) studied one case of lee wave activity over Tasmania. He concluded that the relation used by Fritz (1965) gave a good estimate of mean tropospheric wind speed as a function of the satellite-observed wave length.

Doron and Cohen (1967) investigated lee wave activity in the Middle East. They also found that the parcel method of computing wave lengths yielded a good comparison with satellite-observed wave lengths, but the correspondence of observations with more sophisticated models varied from good to poor. The variation was partially attributed to a lack of more accurate input data required by the complex models.

Some success in relating the turbulent state of the atmosphere to the vertical motions in lee waves has been found by Reiter and Foltz 1967). Based on a combination of lee wave and turbulence theory, he authors have derived a method for forecasting clear air turbulence CAT) over short periods utilizing synoptic charts and satellite-observed ee wave lengths as input data. Although as stated by the investigators, heir method of obtaining the CAT intensities is crude, it does represent

an important step forward in the deduction of the implicit state of the atmosphere from the satellite observations.

According to the above review, it is evident that theoretical models are capable of yielding good estimates of the lee wave length. The simple parcel theory has been verified as a useful tool in relating observed (e. g. by satellite) wave lengths to the mean tropospheric wind speed. These findings reflect the dependence of the lee wave length on the gross wind and stability features of the atmosphere (see Foldvik, 1962). However, when one considers the deduction of the finer structure from satellite pictures, the problem becomes quite complex.

## C. Model Selection and Computational Procedures

In this and the following sections, the feasibility of determining he fine structure of the atmosphere from observations of the larger scale will be investigated. To bridge the gap between these scales of motion, it is necessary to have (a) simultaneous observations on ll scales and (b) a realistic model of the particular phenomenon being onsidered. For lee waves (a) is available from the case studies escribed in an earlier section of this report. However, (b), the vailability of a "realistic" model, raises a number of problems. he comparative theoretical-observational studies discussed previously ndicate that the most important of these are the following:

(1) complex terrain;

(2) wind and temperature soundings that are not synchronized with satellite observations;

(3) wind and temperature soundings removed some distance from the region of lee waves;

(4) unavailability of upwind soundings (e. g. If soundings

are made in the lee of the mountain, they are already contaminated by waves and do not represent the undisturbed state of the atmosphere.);

(5) incomplete observations of the lee wave system and,

(6) the failure of the natural conditions to meet the assumptions of the mathematical idealization.

In the present study, attempts have been made to eliminate, or at least minimize, a number of these problems.

Although the Rockies present the epitome of complex terrain, they do have a number of long north-south ridges, particularly in the vicinity of the observations described earlier. Further, it will be shown that under certain synoptic conditions, it appears that the "effective" surface lies at a considerable distance above the actual surface, thus eliminating the more complex features at lower altitudes.

The wind and temperature soundings utilized for this study, although properly synchronized and located in the lee wave region, suffered from problem (4) listed above. An effort was made to minimize the error through smoothing techniques similar to those suggested by Foldvik (1962).

It is believed that the combined satellite, pillow balloon and photogrammetric observations have described the lee waves in detail, thus allowing a better comparison between observations and theory.

Initially the study will be concerned with a simple model, the purpose being to (a) determine the capability of this model to describe the observed lee wave conditions, (b) isolate the specific conditions under which it applies or breaks down, and (c) on the basis of the latter, select a more realistic model for later studies.

The first model chosen for the computation of lee wave patterns is based on the work of Scorer (1949). The reasons for the selection are the following:

(1) The model is relatively simple, in agreement with the general approach outlined in the last paragraph.

(2) The two layer structure of the model appears to be a good approximation to the real vertical structure of the atmosphere in the cases selected for study.

(3) Since the lenticular clouds that the satellite observes as evidence of lee waves have a tendency to occur near the stable layer in the mid troposphere, it is logical to select a simple model that is most likely to give realistic wave patterns at cloud level. In the cases studied here, the interface of the two layer model always fell in the vicinity of the mid tropospheric stable layer.

Scorer (1949) has extended the work of Lyra (1943) and Queney (1947) for two-dimensional, steady state flow over a small ridge of infinite lateral extent. Allowance for variations of stability and wind speed in the vertical resulted in more realistic lee wave patterns than those produced by earlier models.

Assuming laminar, frictionless and isentropic flow, the basic differential equation derived by Scorer (1949) can be written approximately as

$$\frac{\partial^2 w}{\partial z^2} + (\ell^2 - k^2)w = 0 \ , \qquad (2)$$

where $w$ is the vertical velocity ,

$$\ell^2 = \frac{g\beta}{u^2} - \frac{1}{u}\frac{\partial^2 u}{\partial z^2} \quad , \tag{3}$$

$$\beta = \frac{1}{\theta}\frac{\partial \theta}{\partial z} \quad ,$$

u is the wind component perpendicular to the ridge and

$k = \frac{2\pi}{\lambda}$ , where $\lambda$ is the lee wave length.

This equation is based on further assumptions that the effect of the earth's rotation may be neglected, the disturbance is periodic in x, and the perturbation is small (i. e. non-linear effects are neglected).

Scorer has solved equation (2) by approximating the vertical distribution of $\ell^2$ with two layers such that $\ell_1^2 > \ell_2^2$, where subscripts 1 and 2 apply to the lower and upper layers, respectively. By requiring continuity at the interface of the two layers and demanding that the disturbance should decrease exponentially with height in the upper layer and become zero at the surface, an equation in the lee wave number, k, may be written

$$\mu_1 \coth \mu_1 h + \mu_2 = 0 \quad , \tag{4}$$

where

$$\mu_1 = (k^2 - \ell_1^2)^{1/2} \quad ,$$

$$\mu_2 = (k^2 - \ell_2^2)^{1/2} \quad ,$$

and h is the thickness of the lower layer.

In order to obtain solutions to (4) it is necessary that

$$\ell_1^2 - \ell_2^2 > \frac{\pi^2}{4h^2} \tag{5}$$

The height of the idealized mountain is given by the relation

$$Z_x = \frac{Hb^2}{b^2 + x^2} \tag{6}$$

where $Z_x$ is the height of the terrain at distance x from the center of the mountain ($x = 0$, $Z_x = H$) and b is the half-width parameter, i. e. the horizontal distance from the peak at which $Z_x = H/2$.

By utilizing the Fourier integral theorem and the solution for ζ from equation (4) an approximate solution to (2) is found for the two layer model. The displacement, ζ, of a streamline at height z, is given by the real part of

$$\zeta(z) = \frac{a}{\pi} \frac{f_z(0)}{f_{-h}(0)} \frac{b+ix}{b^2+x^2} + 2ia \frac{f_z(k)}{f'_{-h}(k)} \exp(-kb+ikx) \tag{7}$$

for $x > 0$ and

$$\zeta(z) = \frac{a}{\pi} \frac{f_z(0)}{f_{-h}(0)} \frac{b+ix}{b^2+x^2} \tag{8}$$

for $x < 0$,

where

$x = 0$ is located at the center of the mountain,

$z = 0$ is located at h, the height of the interface between the two layers,

$f_z(k) = \frac{A}{u} (\cosh \mu_1 z - \frac{\mu_2}{\mu_1} \sinh \mu_1 z)$,

A is an arbitrary constant,

$$i = \sqrt{-1} \ ,$$

$$\frac{a}{\pi} = Hb.$$

A prime indicates $\frac{\partial}{\partial z}$ and other symbols are as previously defined.

The computation of the lee wave patterns was accomplished in the following manner:

(1) The pillow balloon tracks for the selected days were extrapolated to the windward side of the Park Range (see Figure 2) with the winds at 500 mb (approximate flight level) nearest in time to the flight. Terrain heights were obtained from United States Geological Survey charts NK 13-10 and NK 13-11, scale 1:250,000. Height data were retrieved at 0, $\pm$ 1/2 and $\pm$ 1 statute mile intervals across the track and at one mile intervals along the track. This procedure was modified slightly along the extrapolated portion of the track to compensate for possible errors in its extension. Here the lateral height values were retrieved at 0, $\pm$ 1 and $\pm$ 2 mile intervals. The height data were subjected to a three-point weighted (1-2-1) running average parallel to the track and a five point weighted (1-2-4-2-1) running average perpendicular to the track. The result is the smoothed terrain profile in which features of horizontal extent less than 1.6 km have been eliminated.

(2) The major terrain features were then fitted with the bell-shaped profile described by equation (6) to yield the necessary H and b parameters.

(3) Since the vertical temperature and wind profiles were measured in the lee of the mountains and thus subjected to modifications by the lee waves, the respective profiles were smoothed. $\ell^2$ was subsequently calculated over 50 mb intervals.

(4) The $\ell^2$ profile was then divided into two layers. The interface (and therefore the depth, h, of the lower layer) was chosen

to coincide approximately with the top of the inversion layer which existed in the mid-troposphere in the two cases selected for study. A mean $\ell^2$ for each layer was determined by weighting each $\ell^2$ value with the thickness of the layer over which it was calculated and averaging the thickness-weighted values throughout the top and bottom layers of the model. $\ell^2$ was only calculated to 300 mb (near an apparent minimum). It was necessary to supplement the Ault wind and temperature data with Denver data in the upper layers (above ~400 mb).

(5) Utilizing the values of h, $\ell_1^2$ and $\ell_2^2$, as determined above, equation (3) was then solved graphically for the lee wave number, k.

(6) Equations (7) and (8) were then solved for the displacements of the streamlines at preselected heights for each mountain peak.

(7) The solutions for the individual peaks were then superimposed. This is a valid step based on the linearity of the model.

## ). Case Studies and Results

The case days chosen for investigation were 9 November 1967 nd 5 January 1968. These selections were made on the basis of the ynoptic flow pattern (wind direction perpendicular to the major ridges) ıd a large quantity of supporting data. The reader is referred to the ɛtailed discussion of the synoptic situation and the observational data an earlier section of this report.

### ıe 9 November 1967 Case

The smoothed mountain profile along the extrapolated track of ɛ pillow balloon launched at 2227 GMT is shown in Figure 18. As indicated on the diagram, the effective surface has been taken as .m rather than the height of North Park or the height of the terrain mediately in the lee of the Rockies.

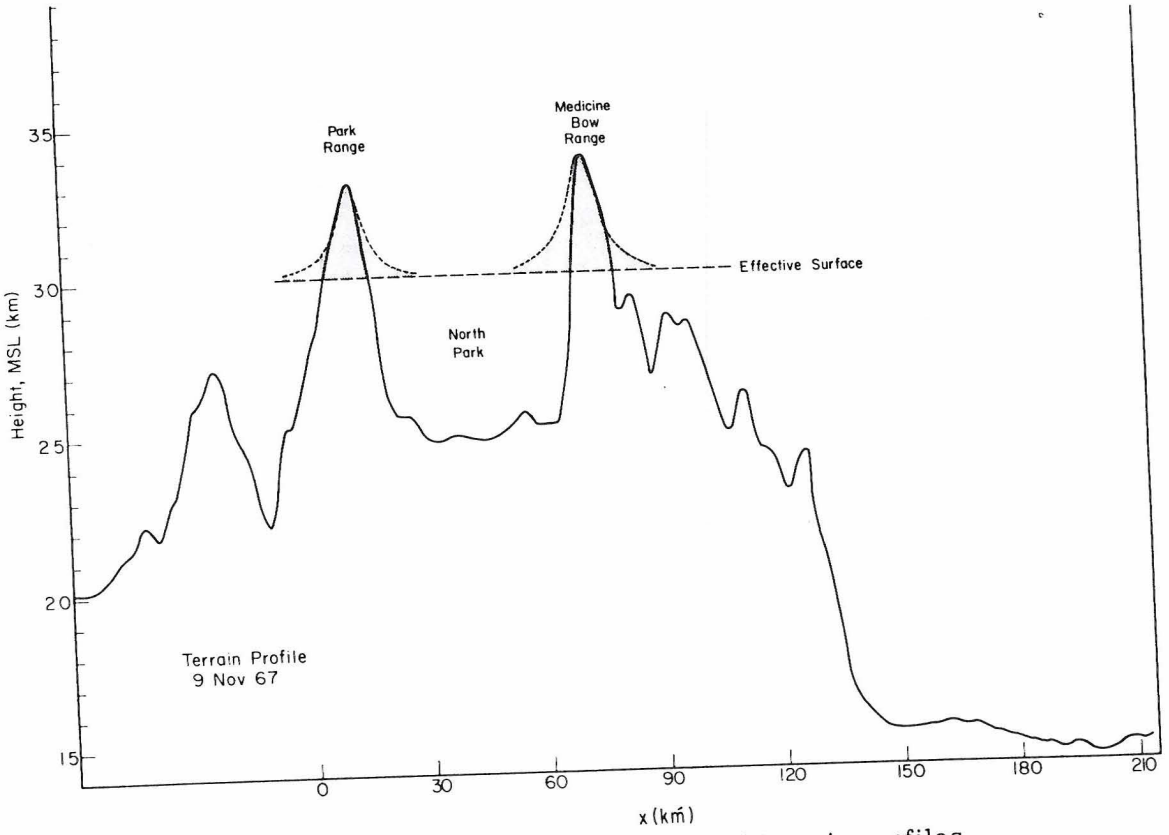


Figure 18. Actual and approximated terrain profiles along pillow balloon trajectory for case 1.

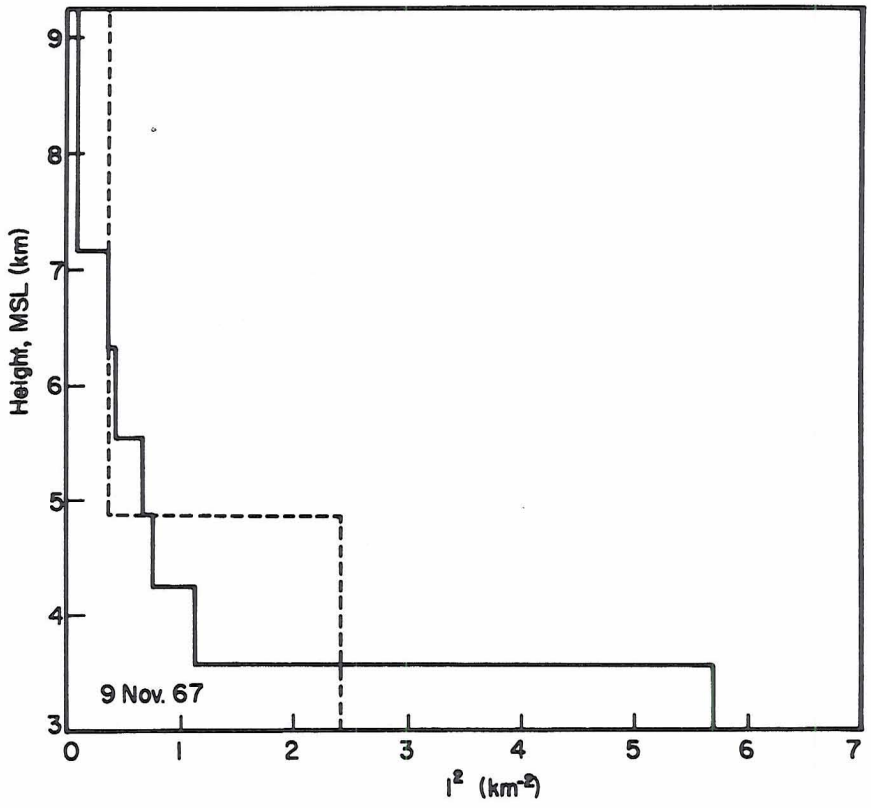


Figure 19. $l^2$ distribution for case 1. Solid line denotes computed distribution, dashed line indicates the two layer approximation.

The problem of specifying the effective surface and thus the effective height of the mountains that give rise to lee waves has been discussed by Döös (1962) and Colquhoun (1966). The decision to use 3 km in the present case was based on the fact that the smoothed Ault wind measurements showed no westerly component below 700 mb. Under these conditions the $\ell^2$ parameter is infinite and lee wave computations are not possible.

The $\ell^2$ profile for the region above 3 km is given in Figure 19. It is evident that a very large decrease in $\ell^2$ occurs between 3.0 and 3.5 km. Sawyer (1960) has computed lee wave patterns under similar conditions. His calculations, based on a quasi-numerical solution of equation (2), demonstrated that the rapid decrease in $\ell^2$ in the lower layers gave rise to very short waves which had little effect on the longer waves at higher levels. This result partially justifies the use of 3 km as the height of the effective surface. The effect of this assumption is that the simplified terrain profile consists of two peaks that are approximated well by equation (6). The result is superposed on the original profile in Figure 18.

The two peaks that make up the simplified profile correspond with the Medicine Bow Range on the east and the Park Range on the west. North of the track the Medicine Bow Range is oriented in a NW-SE direction, while south of the track the range assumes more of a NNW-SSE direction. These orientations may be compared with the approximately E-W track of the pillow balloon in that vicinity. The Medicine Bow Range slopes upward to the south and no major breaks occur between about 15 km north to 20 km south of track. The Park Range, which corresponds with the Continental Divide, runs in an approximately north-south direction with no major break or change in orientation between about 20 km north to 30 km south of track.

Heights, H, and half-width parameters, b, for the peak idealizations are listed in Table 1a. The ratio, H/b, should be small (i. e. of the order of $10^{-1}$) to justify the linearization of the model (see Scorer, 1949; Corby, 1954; Sawyer, 1959). The value of this ratio is about $8 \times 10^{-2}$ for both peaks, apparently meeting the linearization criterion.

The two-layer $\ell^2$ structure, based on the thickness-weighting procedure described earlier is indicated in Figure 19. In the calculation of $\ell^2$ from the smoothed wind and temperature profiles, the effect of the term $-\frac{1}{u}\frac{\partial^2 u}{\partial z^2}$ was found to be small and was therefore neglected.

Input data for the computation of the wave patterns and a summary of observational data available for verification appear in Tables 1a and 1b.

TABLE 1a

| | |
|---|---|
| Date | 9 November 1967 |
| Height of effective surface | 3.0 km |
| h* | 1.85 km |
| $\ell_1^2$ | 2.34 $km^{-2}$ |
| $\ell_2^2$ | 0.31 $km^{-2}$ |
| Terrain Parameters | |
| Park Range | |
| H* | 0.31 km |
| b | 4.0 km |
| Medicine Bow Range | |
| H* | 0.38 km |
| b | 4.8 km |

*height above effective surface

TABLE 1b

9 November 1967

| | Time (GMT) Began | Ended |
|---|---|---|
| Pillow Balloon Flights | 1740 | ~2000 |
| | 2227 | ~0100 |
| Rawinsonde Observations | 1631 | --- |
| | 2008 | --- |
| Ground Photos | 1800 | 1855 |
| Satellite Photographs | 18:21:06 | |
| | 20:11:17 | |

The superposition of the mountain wave patterns produced by the two idealized peaks appears in Figure 20. For the purposes of discussion the pillow balloon flights launched at 1740 and 2227 GMT have been entered on the diagram.

The solution of equation (4), based on the two layer distribution (Figure 19)is 6.2 km. This value may be compared to the apparent 2.5 km wavelengths derived from the ground-based cloud photography and secondary peaks at about 4.6 km in the spectral analysis of the balloon motions.

The most obvious discrepancy in comparing the observed with the computed wave patterns is the inability of the model to describe the amplitudes, particularly in the upper layer. At and below the interface, the computed amplitudes of the shorter wave phenomena appear to be an order of magnitude too small. At the interface (4.85 km) amplitudes of about 25 m were computed, while amplitudes of the shorter wave phenomena occurring in the two pillow balloon flights were estimated to be about 50 to 200 m. This

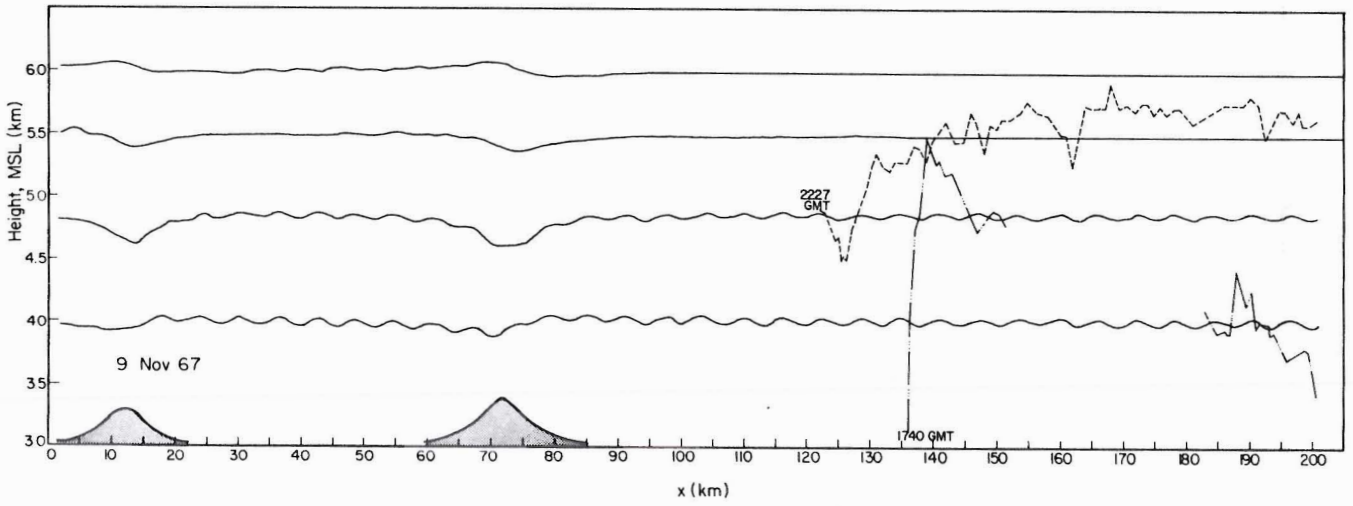


Figure 20. Observed and computed lee wave patterns for case 1. Dashed and dashed-dotted lines indicate pillow balloon flights, solid lines are computed streamlines.

comparison is not completely valid since the greater portion of the balloon paths are located in the upper layer where the ratio of computed to actual amplitudes approaches $10^{-2}$.

The lack of good agreement between observed and computed amplitudes also reflects the arbitrary manner in which the two-layer distribution of $\ell^2$ may be determined from the actual $\ell^2$ profile. Rough calculations have indicated that a variation in the depth, h, of the lower layer could result in a slight (less than an order of magnitude) increase in the amplitudes. This further exemplifies the fact that numerous two-layer distributions of $\ell^2$ could be derived to represent the actual case. On the other hand, the procedure utilized for the selection of the two layers and the subsequent determination of $\ell_1^2$ and $\ell_2^2$ appears to be a logical one and should serve usefully in the evaluation of the model for practical applications. The representativeness of the computed amplitudes is important in the calculation of lee wave energy (e. g. see Reiter and Foltz, 1967) and, at least for this case, it appears that the model amplitudes are too small.

Since, according to the spectral analyses of the pillow balloon data, the actual lee wave pattern consists of the superposition of at least three waves of various lengths and the model depicts only the shorter wave length, any attempt to correlate the theoretical and observed phases is not possible at this point.

Another discrepancy evident in Figure 20 is the large up and downward motion of the balloon at the beginning of the flight. This pattern is comparable to the behavior of theoretical streamlines immediately to the lee of a mountain peak. The location of this phenomenon in Figure 18 indicates that the large vertical movements occurred immediately to the lee of the Rockies and are evidently associated with the rapid decrease in terrain elevation in

that area. It must be concluded, therefore, that the selection of 3 km as the effective surface is artificial and a better description of the terrain is warranted.

Comparison of the wave pattern for each peak with the total pattern indicates that lee waves set up at the Park Range were slightly out of phase with those induced by the Medicine Bow Range, with the result that the total amplitudes were intermediate between the values for the individual peaks. In the immediate vicinity of the Medicine Bow Range, the superposition has caused the streamline pattern to take on a somewhat irregular appearance.

The 5 January 1968 Case

The smoothed topography for the extrapolated balloon track on 5 January 1968 is illustrated in Figure 21. The basic difference between this terrain profile and that for 9 November 1967 is the inclusion of a third major peak, Crown Point, which is only of limited lateral extent. Crown Point corresponds to the northern end of the Mummy Range which is an extensive topographical feature extending over 20 km to the south of the track with a N-S orientation. However, the portion of Crown Point exceeding an elevation of 3 km MSL is limited to about 5 km north of the track.

The effective surface, as indicated in Figure 5, was again selected as 3 km. This selection was based on the presence of a dome of cold air which extended across the Rocky Mountain region. A strong inversion, extending to about 3 km, is evident in the Ault, DEN, and SLC soundings for that day (see Figure 15c). As in the 9 November 1967 case, the $\ell^2$ values (see Figures 22 and 23) were very large below 3 km, decreasing rapidly between 3.0 and 3.5 km.

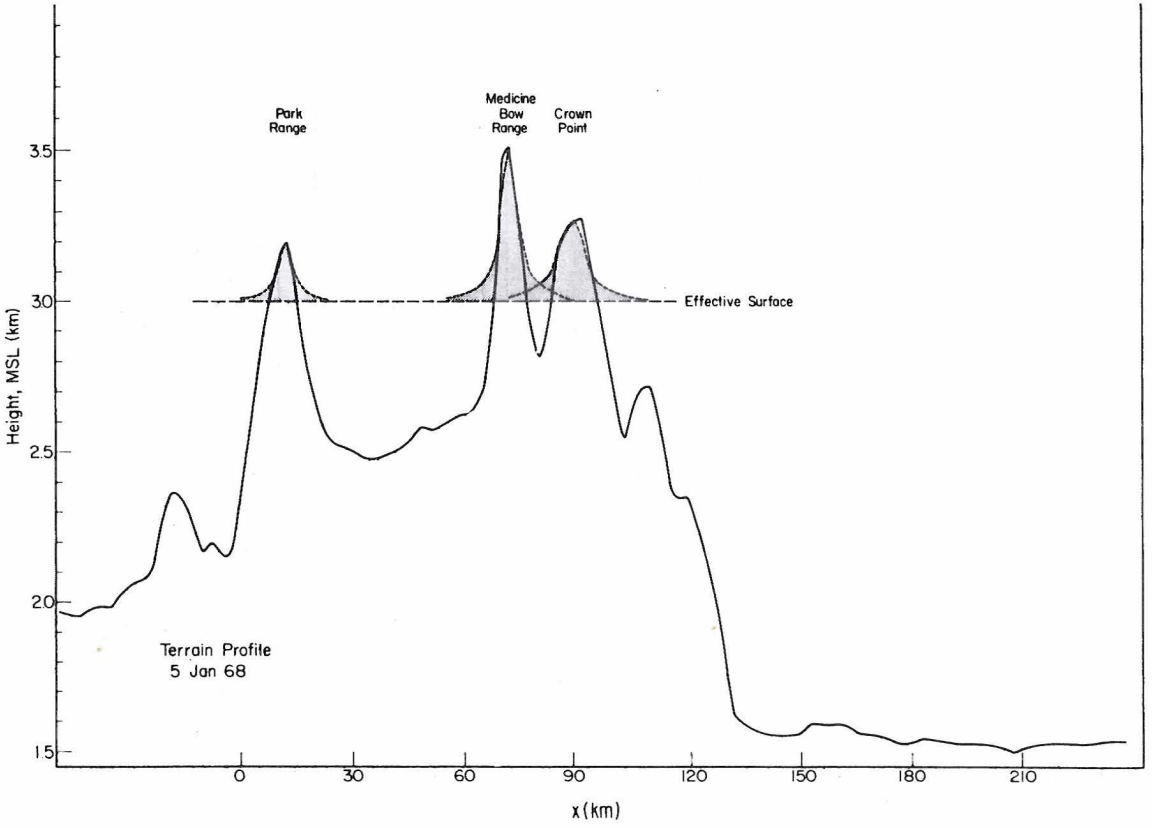


Figure 21. Same as Fig. 18 for cases 2a and 2b.

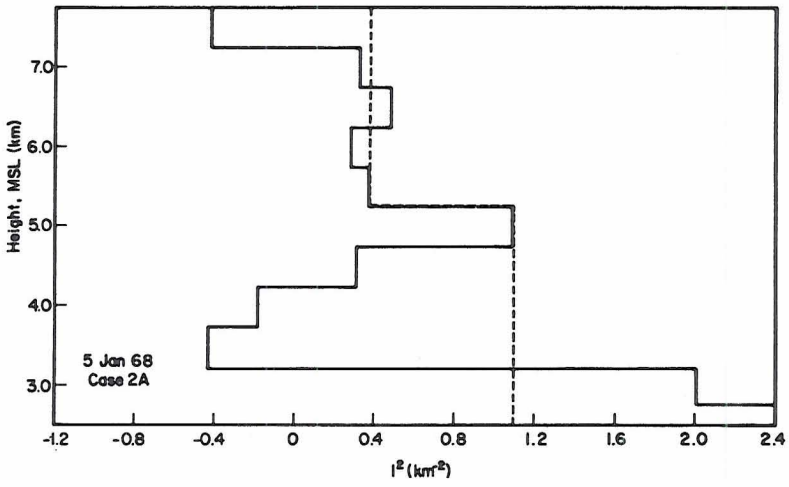


Figure 22. Same as Fig. 19 for case 2a.

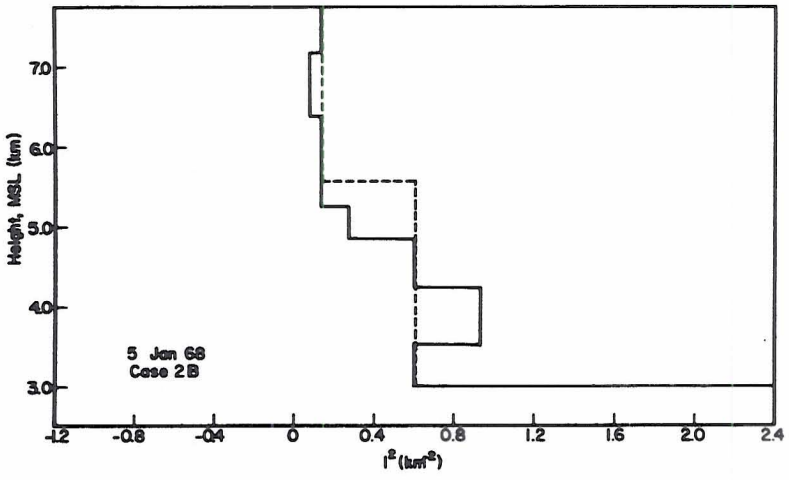


Figure 23. Same as Fig. 19 for case 2b.

The peaks that remain in the simplified profile lend themselves readily to approximation by equation (6). The ratios H/b for the Park Range, the Medicine Bow Range and Crown Point are $0.8 \times 10^{-1}$, $2.0 \times 10^{-1}$, $0.6 \times 10^{-1}$, respectively. These values appear to satisfy the criterion for linearization of the model.

In the present case, $\ell^2$ computations revealed that the term $-\frac{1}{u}\frac{\partial^2 u}{\partial z^2}$ was large. However, the value of the curvature of the wind profile is subject to conjecture due to measurement error (Reiter, 1963) and in the present case due to the use of smoothed lee side soundings. For these reasons, computations of lee wave patterns were performed including that term for case 2a and excluding it for case 2b. Input data for the calculation of wave patterns and a summary of observational data used for verification are listed in Tables 2a and 2b.

TABLE 2a

| Date | 5 January 1968 | |
|---|---|---|
| Case | 2a | 2b |
| Height of the effective surface | 3.0 km | 3.0 km |
| h* | 2.25 km | 2.56 km |
| $\ell_1^2$ | $1.10\ km^{-2}$ | $0.61\ km^{-2}$ |
| $\ell_2^2$ | $0.37\ km^{-2}$ | $0.13\ km^{-2}$ |
| Terrain Parameters | | |
| Park Range | | |
| H* | 0.20 km | 0.20 km |
| b | 2.4 km | 2.4 km |
| Medicine Bow Range | | |
| H* | 0.52 km | 0.52 km |
| b | 2.6 km | 2.6 km |
| Crown Point | | |
| H* | 0.28 km | 0.28 km |
| b | 4.4 km | 4.4 km |

*height above effective surface

TABLE 2b

5 January 1968

| | Time (GMT) | |
|---|---|---|
| | Began | Ended |
| Pillow Balloon Flights | 1603 | ~1820 |
| | 1612 | ~1820 |
| | 1830 | ~2030 |
| Rawinsonde Observation | 2104 | |
| Satellite Photographs | 18:24:38 | |

The $\ell^2$ profiles are illustrated in Figure 22 (case 2a) and Figure 23 (case 2b). The two-layer profile for case 2b was calculated via the thickness weighting procedure described earlier. However, case 2a would not yield a solution with this procedure. Because of the large decrease of $\ell^2$ near 5.25 km, it was decided to use the values of $\ell^2$ immediately above and below this level to represent the upper and lower layers.

Figure 24 illustrates the lee wave pattern derived from the simplified terrain and the two layer approximation of the $\ell^2$ profile for case 2a. Pillow balloon flights during the period are entered on the diagram for comparison purposes. The graphical solution of equation (4) for this case yields a wave length of 9.1 km which may be compared with wave lengths derived from both the spectral analyses (Figures 17 b, c, d, e), nearest peak ~6 km and the radiosonde flight (Figure 17f), nearest wave length is 4 km. The greatest discrepancy, which is immediately obvious from Figure 25, is the poor representation of wave amplitude in the upper layer. In the lower layer, the agreement is slightly better, particularly for the shorter waves. Any correspondence in phase is masked by the

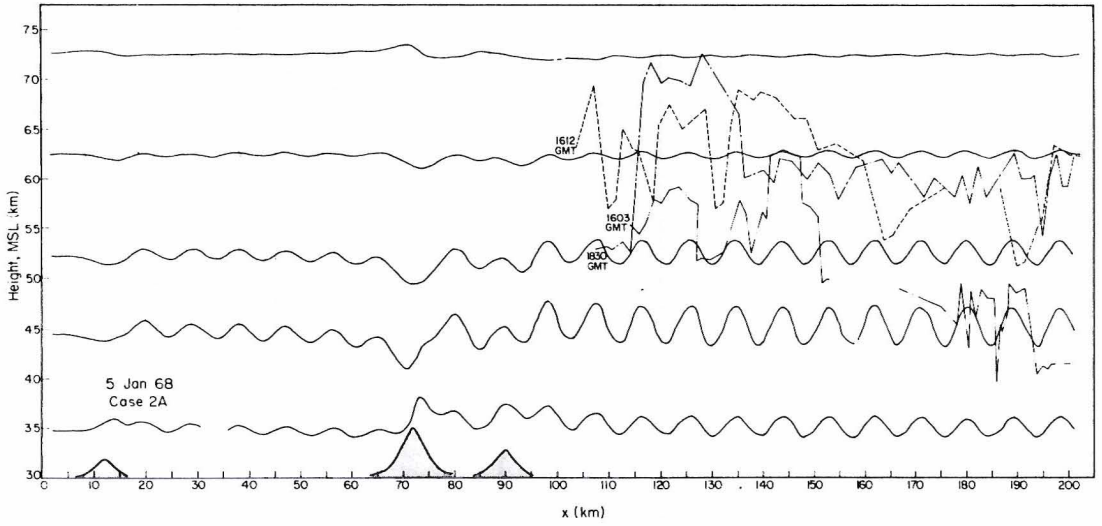


Figure 24. Same as Fig. 20 for case 2a.

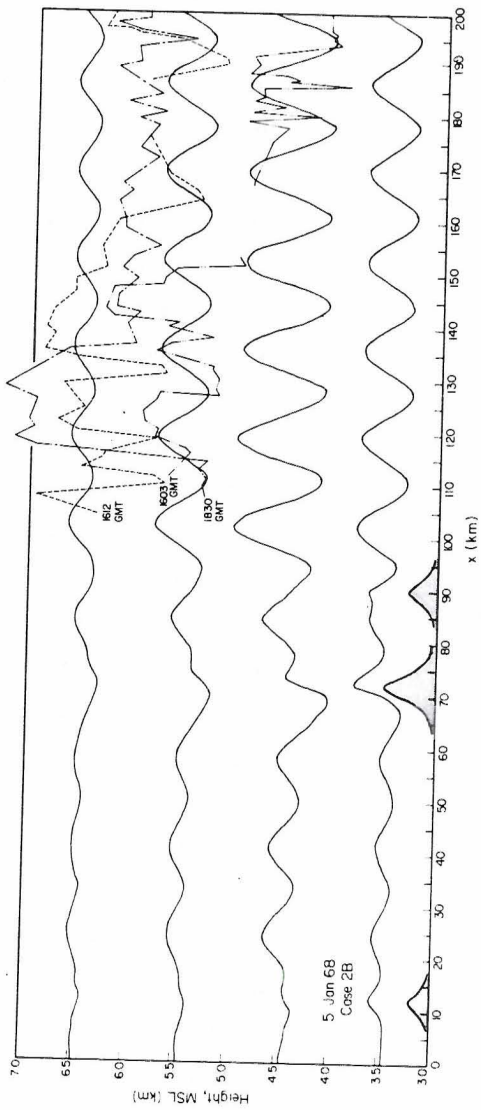


Figure 25. Same as Fig. 20 for case 2b.

existence of longer and shorter waves as shown by the spectral analysis of the pillow balloon flights.

Inspection of the individually computed wave patterns (not shown) of which Figure 24 is the total indicates that the Park Range had a damping effect due to a phase that was exactly opposed to that of the waves induced by the Medicine Bow Range and Crown Point. The latter two reinforced each other, more than compensating for the effect of the Park Range. In the immediate vicinity of the central peak, the wave train set up by the Park Range did act to reinforce the mountain effect (first term in equation (7)) particularly in the streamline near 4.5 km MSL.

The calculated streamline pattern for case 2b appears in Figure 25. The lee wave length is 16.8 km which agrees approximately with the spectral peak at 14 km for the pillow balloon flight launched at 0912 LST. Again, the inability of the model to describe amplitudes in the upper layer is noted, although below the interface the theoretical representation shows better correspondence. The existence of waves of various lengths, as indicated by the spectral analyses of the balloon data (Figures 17 b, c, d, e), precludes a comparison of the phase relationship between the observed and computed waves.

The effects of the theoretical wave trains set up by the individual mountains are similar to case 2a. The Park Range induces a wave train that reinforces the mountain effect immediately to the lee of Crown Point and at the interface of the two layers. Downstream, the lee waves due to the Medicine Bow Range are reinforced by Crown Point while the Park Range has a damping effect. The net result (Figure 25) is that the total amplitude of the lee waves is greater than that of any single component.

In the discussion of the 9 November case, it was noted that the selection of the effective surface appeared to be in error due to the strong downslope motion just to the lee of the Rockies. Although the balloon tracks did not show this phenomenon in the 5 January 1968 case, the possibility exists that the elimination of the layer of strong stability (thus high values of $\ell^2$) in the lower layers through the selection of 3 km as the effective surface may have introduced some error. On this basis, the effective surface for case 2b was reduced to 2.5 km. The result (not shown) was a marked reduction in lee wave amplitude.

At first glance, this result may seem surprising since the mountain heights were increased by more than a factor of two. An analysis of the lee wave amplitude factor in equation (7) was performed in the manner of Corby and Wallington (1956). For simplicity, only the effects of increasing the depth of the lower layer on the lee wave pattern set up by the Medicine Bow Range were considered. The increase in height of the peak, as would be expected, acted to increase the amplitude. This effect, however, was more than compensated for by the decrease in wind speed at the effective surface and the increase in $\ell^2$ in the lower layer. The latter change was primarily due to the greater stability in that region. The total computed effect was a sevenfold decrease in maximum amplitude. These results illustrate the sensitivity of the amplitudes to variations in atmospheric conditions and also indicate that the concept of an "effective surface" may be applicable in some cases.

# CHAPTER V

## SUMMARY AND CONCLUSIONS

The lee wave lengths measured from satellite pictures, by ground-based cloud photogrammetry, and by analysis of super-pressure (pillow) and rawinsonde balloon flights are presented in Table 3. Wave lengths can be approximated from cloud element lengths since the cloud lengths occupy approximately 0.7 to 1.0 wave length.

The wave structure exhibited in cloud patterns in the lee of the Rocky Mountains are a result of the superposition and interaction of waves generated by the topography of the mountains. Since the perturbing influences are of different heights, widths, and lateral extents, and since wind shears and atmospheric stabilities may change along the direction of motion, the waves observed in the lee of the Rockies cannot be expected to be uniform or of a single wave length.

The wave lengths measured on the days shown in Table 3 exhibit a harmonic nature. On October 26, 1967, the wave lengths were approximately 4, 8, and 16 km; on November 9, 2.5, 5, 20, and 40 km; on November 10, 4, 8, and 16 km; and on January 5, 1968, 3, 6, 15, 30, and 60 km. On November 9 and 10, the wave lengths measured from satellite pictures were observed to be fairly uniform over large portions of the western United States. The longer (40 to 60 km) wave length is frequently observed in the region just east of the Rocky Mountains in northeastern Colorado both by satellite and from the ground as a clear area between the wall cloud over the Front Range and upwind edge of the wave cloud at the base of the foothills.

TABLE 3. Lee wave lengths and cloud lengths as measured by satellite, ground-based photographs, superpressure balloons, and rawinsonde balloons

| GMT | Satellite (wave lengths) | Photogrammetry (cloud lengths) | Superpressure balloon spectra (wave lengths) | Rawinsonde (wavelengths) |
|---|---|---|---|---|
| October 26, 1967 | | | | |
| 1625 | | 0.5, 8.0, 8.5 km | | |
| 1650 | | 4.0 km | | |
| 2025 | | 7.0, 7.6, 8.0 km | | |
| 2045 | | 7.0, 7.0 km | | |
| 2232 | | | 4.5, 15.5 km | |
| November 9, 1967 | | | | |
| 1740 | | | 2.2, 4.6 km | |
| 1800 | | 1.9 km | | |
| 18:21:06 | 40 km | | | |
| 1835 | | 1.8 km | | |
| 1855 | | 2.5 km | | |
| 20:11:17 | 15, 18, 25 km | | | |
| 2227 | | | 2.6, 4, 3, 20.5 km | |
| November 10, 1967 | | | | |
| 1735 | | | 3.8, 8.3 km | |
| 1805 | | 6.8, 14 km | | |
| 1840 | | 5.5, 6.0, 6.1, 6.6 km | | |
| 19:17:10 | 15, 17 km | | | |
| 19:11:30 | 17 km | | | |
| 1939 | | | | 4, 16 km |
| 2037 | | | 5.5, 20 km | |
| January 5, 1968 | | | | |
| 1603 | | | 3.2, 5.5, 24 km | |
| 1612 | | | 3.5, 6.3, 14 km | |
| 1830 | | | 6.0, 32 km | |
| Combined | | | 6.0, 27, 60 km | |
| 18:24:38 | 55 km | | | |
| 2104 | | | | 4.0, 33 km |

The harmonic nature of the wavelengths measured in the spectra and verified by ground-based cloud photogrammetry suggest the conversion of kinetic energy to potential energy and the dissipation of turbulent energy toward higher wave numbers at discrete wave-number intervals. Slopes of the spectra reproduced in this report range from "-11/5" to "-5/3", with a dominance of the -11/5 slope.

A comparison of the -11/5 value with turbulence theory reveals that a similar slope was obtained theoretically by Bolgiano (1959) for the so-called "buoyant subrange" of turbulence. At scales of turbulent motion where buoyancy forces are important (scale lengths > 30-100 m) the damping effect of a thermally stratified atmosphere results in turbulent energy dissipation with a spectral slope steeper than -5/3 (i. e., the inertial subrange). It appears that the lee wave lengths and the associated stability conditions observed in the present study generally fulfill the conditions advanced for a buoyant subrange if the waves are assumed to be stationary. Photogrammetric measurements of cloud elements suggest that this assumption is very good for periods of time up to a few hours.

The argument can be advanced that the structure of the atmosphere is determined by the dissipation of turbulent energy in the buoyant subrange because of the temporary conversion of energy in stable layers at certain wave numbers, which in turn are determined by wind shears and stability parameters of the atmosphere and by the underlying topography.

The simultaneous observations of motions on scales from a few tens of meters to over 50 km have presented a unique opportunity to determine the feasibility of deriving the state of the smaller scale structure of the atmosphere from satellite observation of the larger scale. The procedure adopted in the present study was to test the capability of a simple lee wave model to reproduce observed patterns.

Two-dimensional lee wave patterns were computed for a linearized two-layer model. The atmospheric structure was derived from smoothed wind and temperature profiles observed during actual lee wave situations. The terrain profiles were based on smoothed topography along extrapolated pillow balloon tracks. The topography was simplified further by assuming that a strong low level inversion acted to modify the terrain profile in such a way that an "effective surface" could be chosen at the top of the inversion. This approach eliminated complex orographic features in the lower levels and resulted in a small height to half width ratio, H/b. The latter effect fulfilled the linear requirements of the model and thus allowed superposition of the wave trains induced by individual mountains.

The results show that (at least in the two cases studied) fair correspondence exists between observed and computed wave lengths. This finding is in agreement with previous studies and is evidently due to the dependence of the wave length on the large scale characteristics of the $\ell^2$ profile. On the other hand, amplitudes were poorly reproduced. The greatest errors were found in the upper layer where the computed vertical oscillations were too small by an order of magnitude or more. In the lower layer of the model, amplitudes of the correct order of magnitude were found in the 5 January 1968 case. It should be noted that the large lee wave amplitudes in case 2b are in part due to the superposition of solutions. No correlation in phase was noted in either case.

Sources of error may be summarized as follows:

(1) Downstream temperature and wind soundings were already contaminated by lee waves from which the $\ell^2$ profiles were computed.

(2) The inability to measure the term $-\frac{1}{u}\frac{\partial^2 u}{\partial z^2}$ with any confidence casts some doubt on the $\ell^2$ computations.

(3) Although the $\ell^2$ ( $=\frac{g\beta}{u^2}$ ) profiles in both cases showed very large values in the lower layers and values near zero in the upper layers, i.e. apparently a two-layer structure, an exponential decrease of $\ell^2$ with height would have been a better approximation. Under these conditions a model similar to that proposed by Döös (1962) may be applicable.

(4) The selection of an "effective surface" may have eliminated important topographical features. This is especially evident in the 9 November case where strong downward motions were observed in the immediate lee of the Front Range.

(5) Although the Park and Medicine Bow Ranges are good approximations to infinite ridges, Crown Point, which appeared in the 5 January 1968 cases, is of limited lateral extent. It follows that the assumption of two-dimensional flow may not have been applicable.

(6) The pillow balloon tracks may have been contaminated by leaking of the balloons in some cases. Also the fact that balloon positions were recorded at one-minute intervals has led to seemingly erratic vertical oscillations rather than the smooth wave motions that are usually connected with the lee wave phenomenon (e.g. see Reynolds, Lambreth, and Wurtele, 1968). These two effects do not allow an accurate comparison between observed and computed wave motions beyond what has been presented.

(7) The comparison of the balloon tracks with computed wave patterns implies that during the time it took the balloon to traverse the waves the conditions were unchanging and, furthermore, that

the soundings of temperature and wind at some fixed time were representative of these conditions. It appears that these assumptions did not hold in the natural airstream, particularly on 9 November 1967. On this day it took approximately 2 1/2 hours for the balloons to traverse the track plotted on Figure 20. The temperature and wind sounding utilized in the computation of $\ell^2$ was made just prior to the launch of the first pillow balloon flight (see Table 1b for summary of times). Cloud photography indicated rapidly changing wave cloud patterns during a 55-minute period during the flight. Also, the $\ell^2$ distribution (not shown), based on a sounding made just prior to the second pillow balloon flight, gave no lee waves according to the computational procedures outlined previously. These facts imply that the diurnal variations in the atmospheric conditions leading to the actual wave patterns partially account for the discrepancies noted in the 9 November case. Only one sounding was made for the 5 January case and no cloud photographs were taken. Yet the persistence of the stable layer at low levels as shown by Denver and Salt Lake City rawins, suggest that diurnal variations played a smaller role in case 2a and 2b.

The lack of a sufficient number of case studies prohibits definite conclusions in the present study. However, there are indications that under certain conditions a linearized, two-dimensional model may be useful in deriving the characteristics of the mesostructure of the atmosphere from satellite observations. The model treated here appears to be applicable near the interface when the "effective surface" and the depth of the lower layer are properly selected. As mentioned earlier, wave clouds often occur near a mid-tropospheric stable layer which is normally the location of the interface in the two layer model. These statements suggest that the present investigation should be extended to determine whether the simple two layer model is applicable in the vicinity of wave clouds observed by satellite.

Further study is recommended with the following modifications:

(a) upstream temperature soundings should be taken at six-hour intervals;

(b) the position of the pillow balloon should be recorded more frequently (5-10 recordings $min^{-1}$);

(c) longer pillow balloon flights could be made using two M-33 radar installations along the projected flight path;

(d) a temperature sensing device could be added to the transponder;

(e) laminated pillow balloons could be used to reduce the possibility of balloon failure during flight;

(f) more sophisticated models (e.g. Scorer, 1953; Palm and Foldvik, 1960; Döös, 1961) should be considered;

(g) more combined spectral and photogrammetric studies should be made of the harmonic nature of lee waves.

The use of two radar sites, and transponders emitting different frequencies, could allow simultaneous flights at two or three selected altitudes, giving a vertical resolution of the wave nature of the atmosphere. In conjunction with satellite pictures showing the larger distance scales, measurements of phase shifts with height would yield information on the propagation of energy in the atmosphere and on the energetic relationships between the topography of mountains and the atmosphere on the meso- and synoptic scales of motion.

Acknowledgements

The authors wish to acknowledge the guidance of Dr. E. R. Reiter during the research reported here. The analysis of the wave perturbations of the rawinsonde balloons was carried out by Mr. Richard Dirks. The typing was done by Mrs. Sandra Olson and computations by Mr. Thomas Kochneff. The pillow balloon and Ault rawinsonde flights were accomplished by Western Scientific Company under subcontract.

## REFERENCES

Anderson, I. R., 1966: Mountain lee wave activity over Tasmania on 17 April 1966, Australian Meteorological Magazine, 4, 119-131.

Blackman, R. B., and J. W. Tukey, 1958: The Measurement of Power Spectra, Dover Publications Inc., New York, 190 pp.

Bolgiano, R., Jr., 1959: Turbulent spectra in a stably stratified atmosphere, Journal of Geophysical Research, 64, 2226-2229.

Booker, D. R., and L. W. Cooper, 1965: Superpressure balloons for weather research, Journal of Applied Meteorology, 4, 122-129.

Colquhoun, J. R., 1966: An analysis of two occurrences of lee waves, Australian Meteorological Magazine, 14, 158-171.

Conover, J. H., 1964: The identification and significance of orographically induced clouds observed by TIROS satellites, Journal of Applied Meteorology, 3, 226-234.

Corby, G. A., 1954: The airflow over mountains--a review of the state of current knowledge, Quarterly Journal of the Royal Meteorological Society, 20, 491-521.

_____, 1957: Preliminary study of atmospheric waves using radiosonde data, Quarterly Journal of the Royal Meteorological Society, 83, 49-60.

_____, and C. E. Wallington, 1956: Airflow over mountains: the lee wave amplitude, Quarterly Journal of the Royal Meteorological Society, 82, 266-274.

Döös, B. R., 1961: A mountain wave theory including the effect of vertical variation of wind and stability, Tellus, 13, 305-319.

_____, 1962: A theoretical analysis of lee wave clouds observed by TIROS I, Tellus, 14, 301-309.

Goron, E., and A. Cohen, 1967: Mountain lee waves in the Middle East: Theoretical calculations compared with satellite pictures, Final Report under Contract Cwb-11055, Department of Meteorology, Hebrew University of Jerusalem, 12 pp.

Goldvik, A., 1962: Two-dimensional mountain waves--a method for rapid computations of lee wave lengths and vertical velocities, Quarterly Journal of the Royal Meteorological Society, 88, 271-285.

Fritz, S., 1965: The significance of mountain lee waves as seen from satellite pictures, Journal of Applied Meteorology, 4, 31-37.

Hayman, R.W., and J.A. Peterka, 1963: Feasibility of balloon trajectory analysis utilizing analytical photogrammetry, Atmospheric Science Technical Paper No. 45, Colorado State University, 17 pp.

Krishnamurti, T.N., 1964: Theory of two-dimensional mountain waves, Reviews of Geophysics, 2, 593-624.

Lally, V.E., 1967: Superpressure balloons for horizontal soundings of the atmosphere, NCAR-TN-28, National Center for Atmospheric Research, Boulder, Colorado, 44-45.

Lyra, G., 1943: Theorie des stationaren Leewellenströmung in freier Atmosphäre, Zeitschrift für angewandte Mathematik und Mechanik, 32, 1-28.

Neumann, R., 1967: Meteorological satellite data--final report of studies, The Hebrew University of Jerusalem, Jerusalem, 10 pp.

Palm, E., and A. Foldvik, 1960: Contribution to the theory of two-dimensional mountain waves, Geofysiske Publikasjoner, 6, 1-29.

Queney, P., 1947: Theory of perturbations in stratified currents with application to airflow over mountain barriers, Miscellaneous Report 23, University of Chicago Press.

Reed, D.G., 1952: Standing waves, Australian Meteorological Magazine, 2, p. 27.

Reiter, E.R., 1963: Jet Stream Meteorology, University of Chicago Press, Chicago and London, 515 pp.

_____, and H.P. Foltz, 1967: The prediction of clear air turbulence over mountainous terrain, Journal of Applied Meteorology, 6, 549-556.

_____, and R.W. Hayman, 1962: On the nature of clear-air turbulence (CAT), Atmospheric Science Technical Paper No. 28, Colorado State University, 40 pp.

Reynolds, R. D., R. L. Lambreth, and M. G. Wurtele, 1968: Investigation of a complex mountain situation, Journal of Applied Meteorology, 7, 353-358.

Sawyer, J. S., 1959: The introduction of the effects of topography into methods of numerical forecasting, Quarterly Journal of the Royal Meteorological Society, 85, 31-43.

_____, 1960: Numerical calculations of displacements of a stratified airstream crossing a ridge of small height, Quarterly Journal of the Royal Meteorological Society, 86, 326-345.

Scorer, R. S., 1949: The theory of waves in the lee of mountains, Quarterly Journal of the Royal Meteorological Society, 75, 41-56.

_____, 1953: Theory of airflow over mountains: II - The flow over a ridge, Quarterly Journal of the Royal Meteorological Society, 79, 70-83.

Widger, W. K., P. E. Sherr, and C. W. C. Rogers, 1965: Practical interpretation of meteorological satellite data, Final Report, Contract AF 19(628)-2471, 380 pp.